Title: $CD8^+$ T cells in lymphoid tissues exhibit distinct functional and transcriptional signatures that associate with elite control of HIV

Summary: Elite control of HIV replication is associated with polyfunctional lymphoid memory $CD8^+$ T cells that lack overt cytolytic activity and home to B cell follicles.

Authors: Son Nguyen[1], Claire Deleage[2], Samuel Darko[3], Amy Ransier[3], Duc Truong[4], Divyansh Agarwal[5], Alberto Sada Japp[1], Vincent H. Wu[1], Leticia Kuri-Cervantes[1], Mohamed Abdel-Mohsen[6], Perla M. Del Rio Estrada[7], Yuria Ablanedo-Terrazas[7], Emma Gostick[8], James A. Hoxie[9], Nancy R. Zhang[5], Ali Naji[10], Gustavo Reyes-Terán[7], Jacob D. Estes[11,12], David A. Price[8], Daniel C. Douek[3], Steven G. Deeks[13], Marcus Buggert[14*], Michael R. Betts[1*#]

Affiliations: [1]Department of Microbiology, Perelman School of Medicine, University of Pennsylvania, Philadelphia, PA 19104, USA; [2]AIDS and Cancer Virus Program, Frederick National Laboratory for Cancer Research, Leidos Biomedical Research, Inc., Frederick, MD 21702, USA; [3]Human Immunology Section, Vaccine Research Center, National Institute of Allergy and Infectious Diseases, National Institutes of Health, Bethesda, MD 20892, USA; [4]Department of Mathematics, Southern Methodist University, Dallas, TX 75205, USA; [5]Department of Statistics, University of Pennsylvania, Philadelphia, PA 19104, USA; [6]The Wistar Institute, Philadelphia, PA 19104, USA; [7]Departamento de Investigación en Enfermedades Infecciosas, Instituto Nacional de Enfermedades Respiratorias, Mexico City 14080, Mexico; [8]Division of Infection and Immunity, Cardiff University School of Medicine, Cardiff CF14 4XN, UK; [9]Department of Medicine, Perelman School of Medicine, University of Pennsylvania, Philadelphia, PA 19104, USA; [10]Department of Surgery, Perelman School of

Medicine, University of Pennsylvania, Philadelphia, PA 19104, USA; [11]Vaccine and Gene Therapy Institute, Oregon Health and Science University, Portland, OR 97239, USA; [12]Division of Pathobiology and Immunology, Oregon National Primate Research Center, Oregon Health and Science University, Portland, OR 97239, USA; [13]Department of Medicine, University of California, San Francisco General Hospital, San Francisco, CA 94110, USA; [14]Department of Medicine Huddinge, Karolinska Institutet, Karolinska University Hospital Huddinge, 14186 Stockholm, Sweden.

[*]These authors contributed equally

[#]Corresponding author

Highlighted text indicates changes from the previously submitted manuscript

ABSTRACT

The functional properties of circulating $CD8^+$ T cells have been associated with immune control of HIV. However, viral replication occurs predominantly in secondary lymphoid tissues, such as lymph nodes (LNs). We used an integrated single-cell approach to characterize effective HIVspecific $CD8^+$ T cell responses in the LNs of elite controllers (ECs), defined as individuals who suppress viral replication to extremely low levels in the absence of antiretroviral therapy (ART). Higher frequencies of total memory and follicle-homing HIV-specific $CD8^+$ T cells were detected in the LNs of ECs compared with the LNs of chronic progressors (CPs). Moreover, HIV-specific $CD8^+$ T cells potently suppressed viral replication without demonstrable cytolytic activity in the LNs of ECs, which harbored substantially lower amounts of $CD4^+$ T cell-associated HIV DNA and RNA compared with the LNs of CPs. Single-cell RNA sequencing (scRNAseq) analyses further revealed a distinct transcriptional signature among HIV-specific $CD8^+$ T cells from the LNs of ECs, typified by the downregulation of inhibitory receptors and cytolytic molecules and the upregulation of multiple cytokines, predicted secreted factors, and components of the protein translation machinery. Collectively, these results provide a mechanistic framework to expedite the identification of novel antiviral factors, highlighting a potential role for the localized deployment of non-cytolytic functions as a determinant of immune efficacy against HIV.

INTRODUCTION

AIDS is a persistent global health issue with no existing vaccine or cure. Most individuals infected with HIV experience high levels of ongoing viral replication, leading to a progressive loss of $CD4^+$ T cells and disease onset in the absence of antiretroviral therapy (ART). However, a small subset of HIV-infected individuals (< 1%), termed elite controllers (ECs), spontaneously control viral replication below the limit of detection and generally do not progress to AIDS. It is established that virus-specific $CD8^+$ T cells are critical determinants of the EC phenotype in humans and rhesus macaques *(1, 2)*. In addition, HIV-specific $CD8^+$ T cells in ECs are qualitatively distinct from HIV-specific $CD8^+$ T cells in chronic progressors (CPs), typically displaying enhanced polyfunctionality *(3, 4)*, cytolytic activity *(5-7)*, and proliferative capacity *(5, 8)*, as well as a more differentiated memory phenotype and a characteristic specificity profile *(4, 9-11)*. These attributes have been documented primarily among circulating lymphocytes, however, whereas HIV replication occurs predominantly in lymphoid tissues (LTs) *(12-15)*.

LTs are major reservoir sites for HIV. Recent studies have further demonstrated that almost 99% of viral RNA $(vRNA)^+$ cells in SIV-infected rhesus macaques occur in LTs *(16)*, reinforcing the need to understand anatomically colocalized mechanisms of immune control. It has long been known that circulating $CD8^+$ T cells are more cytolytic than $CD8^+$ T cells in the LTs of donors infected with HIV *(17)*. Moreover, a state of immune privilege exists in LTs, which limits immunosurveillance by cytolytic HIV-specific $CD4^+$ and $CD8^+$ T cells *(18, 19)*. In conjunction with the identification of distinct LT-resident memory $CD8^+$ T cell subsets *(20-22)*, these observations suggest that HIV-specific $CD8^+$ T cells limit viral replication in LTs via effector mechanisms that differ from those employed by circulating HIV-specific $CD8^+$ T cells *(22)*. It

also seems reasonable to propose that non-cytolytic suppression rather than cytolytic eradication dictates effective immune control of HIV, given reports of ongoing viral evolution *(23, 24)* and the presence of replication-competent viral strains in ECs *(25)*. However, this proposition remains unproven to date, because previous studies have not defined the antiviral efficacy and functional characteristics of HIV-specific $CD8^+$ T cells in the LTs of ECs.

In this study, we used a variety of methodological approaches, including polychromatic flow cytometry and single-cell RNA sequencing (scRNAseq) analyses, to compare the functional and transcriptional properties of HIV-specific $CD8^+$ T cells in the peripheral blood and lymph nodes (LNs) of ECs and CPs. Our findings demonstrate that immune control of viral replication is associated with the occurrence of polyfunctional HIV-specific memory $CD8^+$ T cells that exhibit a weak cytolytic signature and preferentially home to B cell follicles in the LNs of ECs.

RESULTS

$CD8^+$ T cells actively suppress HIV replication in the LNs of ECs

To define the nature of protective $CD8^+$ T cell responses in LNs, where HIV replicates *in vivo*, we obtained tissue biopsies (cervical, iliac, inguinal, mesenteric, pelvic, or peribronchial LNs) and fine needle aspirates (inguinal LNs) from HIV^+ individuals on antiretroviral therapy (ART) and untreated HIV^+ individuals categorized as acute seroconverters, ECs, or CPs (**Supplementary Table 1**). Extremely low levels of $vRNA^+$ cells were detected in the LNs of ECs compared with the LNs of CPs ($p = 0.0174$, **Fig. 1a**). In line with previous findings *(26)*, $vRNA^+$ cells were visualized in the B cell follicles and the paracortical region (T cell zone) (**Supplementary Fig. 1**). Total $CD4^+$ T cell-associated HIV DNA and RNA measurements were

also lower in the LNs of ECs compared with the LNs of CPs ($p = 0.0428$ and $p = 0.0016$, respectively, **Fig. 1b**), and $CD8^+$ T cells from the LNs of ECs displayed greater efficacy in a modified viral suppression assay *(27)* compared with $CD8^+$ T cells from the LNs of CPs ($p = 0.0224$) and $CD8^+$ T cells from the LNs of HIV^+ individuals on ART ($p = 0.0323$, **Fig. 1c**). These results suggest that $CD8^+$ T cells maintain active control of HIV replication in the LNs of ECs.

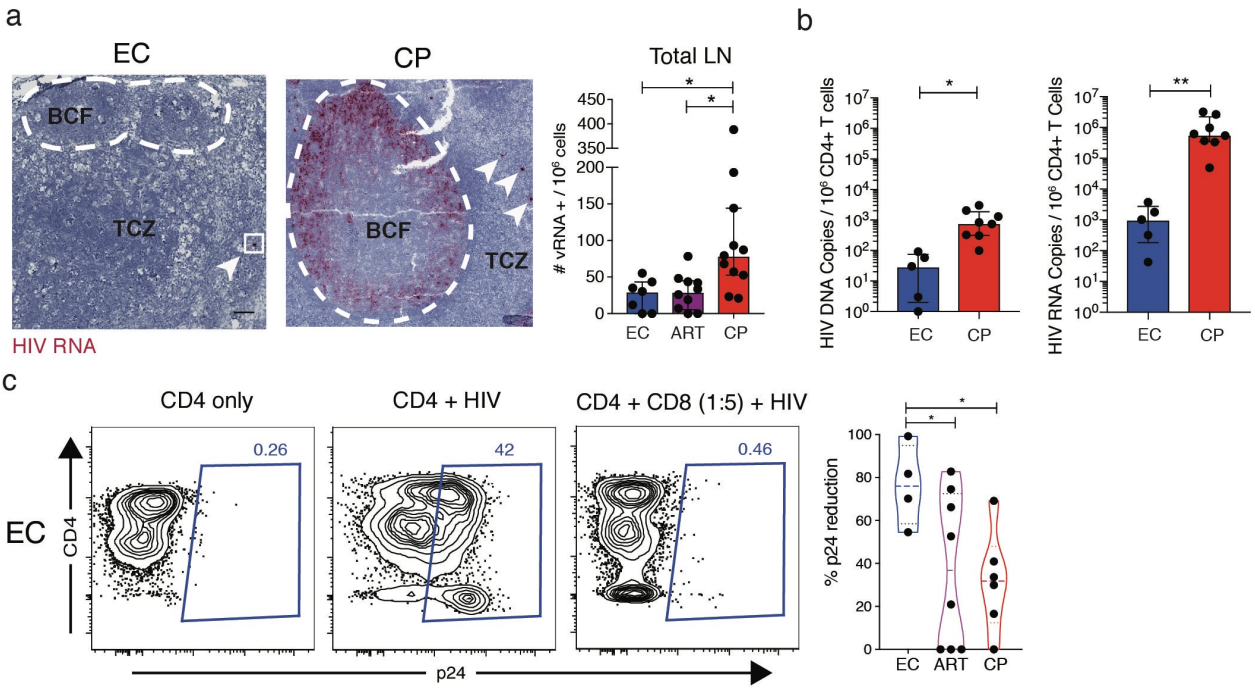

$CD8^+$ T cells exhibit weak cytolytic activity in the LNs of ECs

In peripheral blood, the frequency of cytolytic HIV-specific $CD8^+$ T cells, defined by expression of perforin and granzyme B, correlates inversely with plasma viral load (pVL) *(5-7)*. We therefore hypothesized that enhanced $CD8^+$ T cell-mediated cytolytic activity may underlie viral control in the LNs of ECs. However, lower frequencies of perforin$^+$, granzyme B$^+$, and perforin$^+$ granzyme B$^+$ memory $CD8^+$ T cells were detected in the LNs of ECs compared with the LNs of CPs ($p = 0.0001$, $p = 0.0025$, and $p = 0.0003$, respectively, **Fig. 2a** and **Supplementary Fig. 2a,b**). The frequency of perforin$^+$ granzyme B$^+$ memory $CD8^+$ T cells also correlated positively

with pVL ($r = 0.8213$, $p < 0.0001$, **Fig. 2b**). Importantly, perforin and granzyme B were highly expressed among circulating memory $CD8^+$ T cells in donor-matched samples from ECs, indicating that the non-cytolytic phenotype was restricted to LNs (**Supplementary Fig. 2c**). Immunohistochemical analyses confirmed that fewer perforin$^+$ $CD8^+$ T cells, but not granzyme B^+ $CD8^+$ T cells, were present in the LNs of ECs compared with the LNs of CPs (**Fig. 2c,d**).

We then used human leukocyte antigen (HLA) class I-matched tetramers to examine HIV-specific $CD8^+$ T cells. Higher frequencies of tetramer$^+$ $CD8^+$ T cells were present in the LNs of ECs compared with the LNs of CPs ($p = 0.04$) (**Fig. 2e**). However, these HIV-specific $CD8^+$ T cells expressed very low levels of perforin and granzyme B, especially in the LNs of ECs (**Fig. 2f**). In response to cognate peptide stimulation, HIV-specific $CD8^+$ T cells from the LNs of ECs also failed to upregulate either perforin or granzyme B, unlike $CD8^+$ T cells paired by donor and specificity from the peripheral blood of ECs (**Supplementary Fig. 3a**). Moreover, $CD8^+$ T cells from the LNs of ECs did not exhibit discernable expression of perforin or granzyme B after 3 days in culture with HIV-infected $CD4^+$ T cells from the same LNs (**Supplementary Fig. 3b**).

To quantify rather than infer cytolytic activity, we performed *ex vivo* redirected killing assays based on the detection of active caspase 3, which reliably identified non-viable target cells (**Supplementary Fig. 4a,b**). In contrast to circulating $CD8^+$ T cells, donor-matched $CD8^+$ T cells from the LNs of ECs largely failed to kill P815 mastocytoma target cells pre-coated with a CD3-specific monoclonal antibody, which mimics signals delivered via the TCR (**Fig. 2g**). A similar anatomical discrepancy was observed using paired samples from CPs (**Fig. 2g**). Moreover, no

significant increases in target cell death were observed after extended incubation (24 hours), ruling out the involvement of temporally delayed killing mechanisms (**Supplementary Fig. 4b**).

Collectively, these data suggest that cytolytic activity does not contribute mechanistically to the protective attributes of $CD8^+$ T cells in the LNs of ECs.

$CD8^+$ T cells display increased follicle-homing potential in the LNs of ECs

B cell follicles are thought to represent immunoprivileged sites that potentiate HIV persistence as a consequence of limited immunosurveillance by $CD8^+$ T cells *(2, 28-31)*. Previous studies have also demonstrated an inverse correlation between the frequency of follicle-homing ($CXCR5^+$) $CD8^+$ T cells and pVL *(18, 32, 33)*. In line with these findings and the relative absence of $vRNA^+$ cells in the B cell follicles of ECs (**Fig. 1b**), we detected higher frequencies of $CXCR5^+$ memory $CD8^+$ T cells in the LNs of ECs compared with the LNs of CPs ($p = 0.0288$, **Fig. 2h**). A similar trend was observed for HIV-specific $CXCR5^+$ $CD8^+$ T cells ($p = 0.124$, **Fig. 2i**). However, perforin and granzyme B were typically expressed at higher frequencies among $CXCR5^-$ $CD8^+$ T cells compared with $CXCR5^+$ $CD8^+$ T cells, reaching significance in the ART cohort ($p = 0.0026$, **Fig. 2j**).

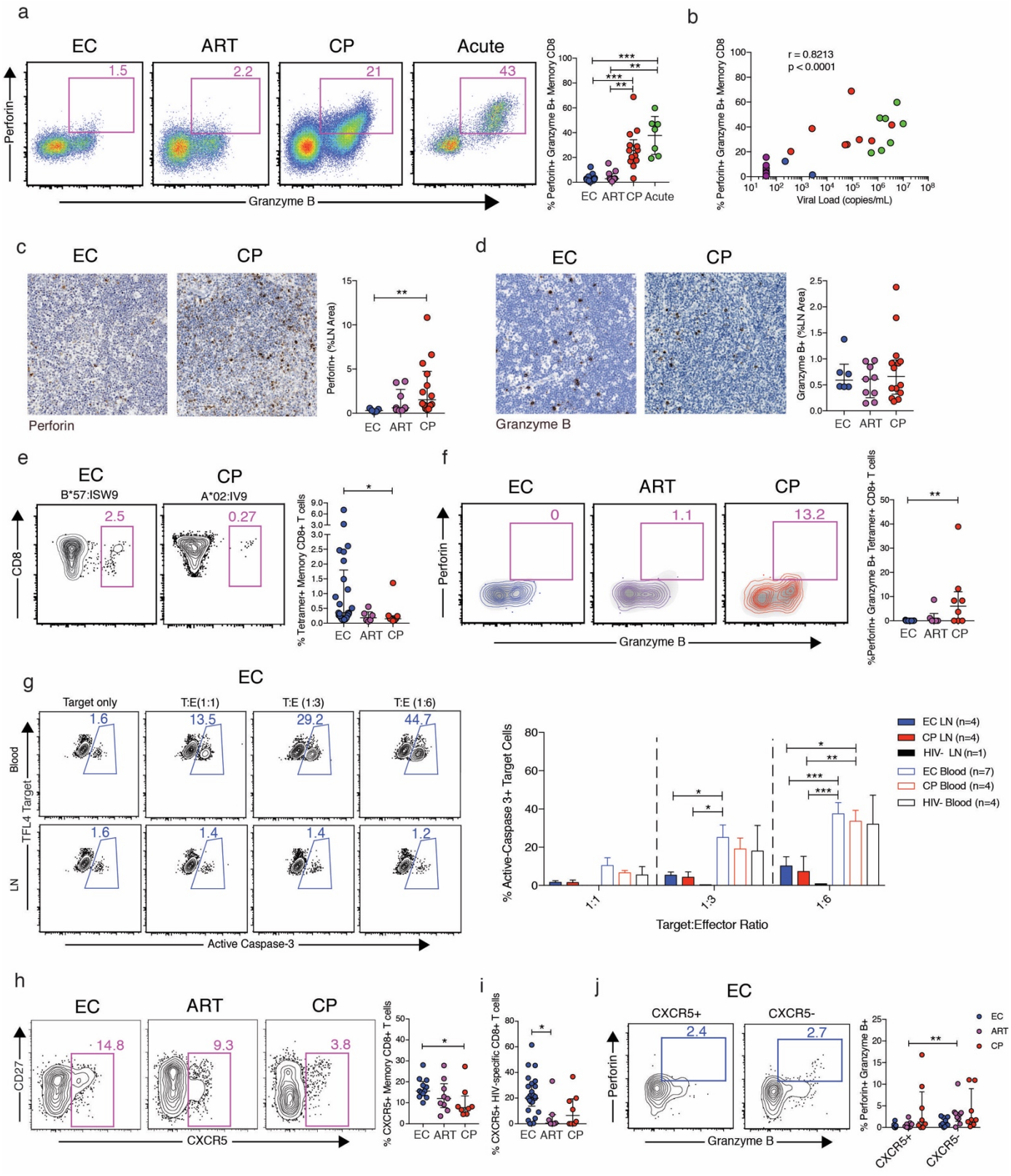
a
EC
ART
CP
Acute
1.5
2.2
21
43
Perforin
Granzyme B
% Perforin+ Granzyme B+ Memory CD8
EC ART CP Acute
b
r = 0.8213
p < 0.0001
% Perforin+ Granzyme B+ Memory CD8
Viral Load (copies/mL)
c
EC
CP
Perforin
Perforin+ (%LN Area)
EC ART CP
d
EC
CP
Granzyme B
Granzyme B+ (%LN Area)
EC ART CP
e
EC
CP
B*57:ISW9
A*02:IV9
2.5
0.27
CD8
% Tetramer+ Memory CD8+ T cells
EC ART CP
f
EC
ART
CP
0
1.1
13.2
Perforin
Granzyme B
%Perforin+ Granzyme B+ Tetramer+ CD8+ T cells
EC ART CP
g
EC
Target only
T:E(1:1)
T:E (1:3)
T:E (1:6)
1.6
13.5
29.2
44.7
1.6
1.4
1.4
1.2
Blood
TFL4 Target
LN
Active Caspase-3
% Active-Caspase 3+ Target Cells
Target:Effector Ratio
1:1
1:3
1:6
EC LN (n=4)
CP LN (n=4)
HIV- LN (n=1)
EC Blood (n=7)
CP Blood (n=4)
HIV- Blood (n=4)
h
EC
ART
CP
14.8
9.3
3.8
CD27
CXCR5
% CXCR5+ Memory CD8+ T cells
EC ART CP
i
% CXCR5+ HIV-specific CD8+ T cells
EC ART CP
j
EC
CXCR5+
CXCR5-
2.4
2.7
Perforin
Granzyme B
% Perforin+ Granzyme B+
EC
ART
CP
CXCR5+
CXCR5-

HIV-specific CD8$^+$ T cells have a distinct transcriptional profile in the LNs of ECs

To identify potential correlates of viral control in LTs, we analyzed the transcriptomes of resting HIV-specific CD8$^+$ T cells from the LNs of ECs and CPs (**Fig. 3a**). The scRNAseq data were initially processed using an unsupervised kernel-based algorithm to determine cellular similarity in a global and unbiased manner (see **Materials and Methods**). Clusters of transcriptionally distinct cells were present in each donor group (**Fig. 3b**). Importantly, normalized expression levels of *PRF1* and *GZMB* were lower in HIV-specific CD8$^+$ T cells from the LNs of ECs compared with HIV-specific CD8$^+$ T cells from the LNs of CPs (**Fig. 3c**), and normalized expression levels of transcripts encoding other cytolytic molecules, including *GZMA*, *GZMH*, *GZMK*, *GZMM*, *FASL*, and *TNFSF10 (34, 35)*, were either comparable between groups or enriched in HIV-specific CD8$^+$ T cells from the LNs of CPs compared with HIV-specific CD8$^+$ T cells from the LNs of ECs (**Fig. 3c**).

We then applied a supervised machine-learning algorithm to determine which transcripts best characterized HIV-specific CD8$^+$ T cells from the LNs of ECs and HIV-specific CD8$^+$ T cells from the LNs of CPs (see **Materials and Methods**). A set of 200 genes reliably distinguished each donor group (average error < 0.5%) (**Fig. 3d**). Hierarchical clustering of these 'feature' genes clarified the key inter-group differences (**Fig. 3e**), most of which could be assigned to immune response pathways via gene ontology (GO) analysis (**Fig. 3f**), and t-Distributed Stochastic Neighbor Embedding (tSNE) visualization generated two distinct clusters of HIV-specific CD8$^+$ T cells that clearly differentiated ECs from CPs (**Fig. 3g**). Overlaying transcript levels of specific 'feature' genes onto the tSNE plot further revealed that HIV-specific CD8$^+$ T

cells from the LNs of CPs preferentially expressed inhibitory receptors, such as *TIGIT*, *LAG3*, *CD244,* as well as the terminal differentiation marker *KLRG1* and the transcription factor *EOMES*, collectively indicating an exhausted phenotype *(36-38)*, whereas HIV-specific $CD8^+$ T cells from the LNs of ECs preferentially expressed *IL7R,* which is crucial for homeostasis *(39)*, and several chemokines/cytokines, such as *CCL5* and *IL32*, collectively indicating a highly functional memory phenotype (**Fig. 3g**).

To confirm and extend these findings, we reanalyzed our scRNAseq data using the reproducibilityoptimized test statistic (ROTS) *(40)*, a Bayesian model of differential distribution (scDD) *(41)*, and Seurat *(42)*. A total of 2,264 differentially expressed genes achieved significance in at least two of these independent analytical frameworks (**Supplementary Fig. 5a and Supplementary Table 2**). These genes were enriched for immune-related terms, such as 'immune response', 'immune system process', and 'defense response', in GO analyses (**Supplementary Fig. 5b**). Of particular note, ingenuity pathway analysis (IPA) further identified a core cassette of 11 transcripts encoding predicted secreted factors that were selectively upregulated in HIV-specific $CD8^+$ T cells from the LNs of ECs, including *TNF*, *CCL5, RNASE1*, and *IL32*, which have been shown to suppress HIV replication *(43-49)* (**Supplementary Fig. 5c**).

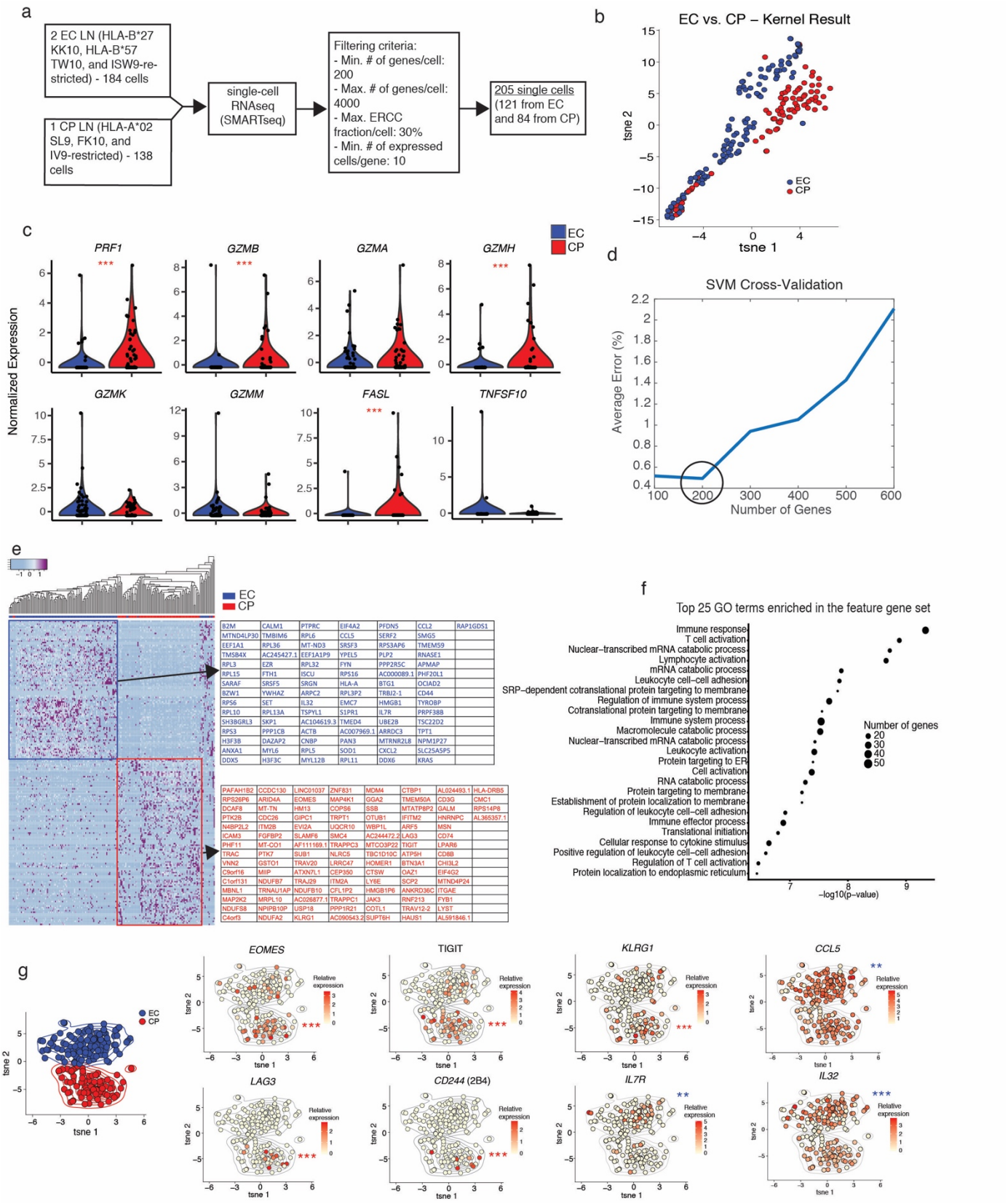
a
2 EC LN (HLA-B*27 KK10, HLA-B*57 TW10, and ISW9-restricted) - 184 cells
1 CP LN (HLA-A*02 SL9, FK10, and IV9-restricted) - 138 cells
single-cell RNAseq (SMARTseq)
Filtering criteria:
- Min. # of genes/cell: 200
- Max. # of genes/cell: 4000
- Max. ERCC fraction/cell: 30%
- Min. # of expressed cells/gene: 10
205 single cells (121 from EC and 84 from CP)
b
EC vs. CP – Kernel Result
tsne 2
tsne 1
EC
CP
c
PRF1
GZMB
GZMA
GZMH
GZMK
GZMM
FASL
TNFSF10
Normalized Expression
d
SVM Cross-Validation
Average Error (%)
Number of Genes
e
EC
CP
f
Top 25 GO terms enriched in the feature gene set
Immune response
T cell activation
Nuclear−transcribed mRNA catabolic process
Lymphocyte activation
mRNA catabolic process
Leukocyte cell−cell adhesion
SRP−dependent cotranslational protein targeting to membrane
Regulation of immune system process
Cotranslational protein targeting to membrane
Immune system process
Macromolecule catabolic process
Nuclear−transcribed mRNA catabolic process
Leukocyte activation
Protein targeting to ER
Cell activation
RNA catabolic process
Protein targeting to membrane
Establishment of protein localization to membrane
Regulation of leukocyte cell−cell adhesion
Immune effector process
Translational initiation
Cellular response to cytokine stimulus
Positive regulation of leukocyte cell−cell adhesion
Regulation of T cell activation
Protein localization to endoplasmic reticulum
Number of genes
−log10(p−value)
g
EC
CP
EOMES
TIGIT
KLRG1
CCL5
LAG3
CD244 (2B4)
IL7R
IL32
Relative expression
tsne 1
tsne 2

HIV-specific CD8$^+$ T cells are polyfunctional and translate proteins efficiently in the LNs of ECs

In response to cognate peptide stimulation, higher frequencies of HIV-specific CD8$^+$ T cells from the LNs of ECs produced TNF compared with HIV-specific CD8$^+$ T cells from the LNs of CPs ($p = 0.0003$) and HIV-specific CD8$^+$ T cells from the LNs of HIV$^+$ individuals on ART ($p = 0.039$) (**Fig. 4a**,**b**). A similar trend was observed for IFNγ, MIP-1β, and IL-2 (**Fig 4b**). Moreover, HIV-specific CD8$^+$ T cells from the LNs of ECs were frequently polyfunctional, whereas HIV-specific CD8$^+$ T cells from the LNs of CPs were predominantly monofunctional (**Fig. 4c**,**d**).

To seek an explanation for these findings, we returned to our GO analysis of the 200 'feature' genes. In addition to immune-related terms, several protein translation-related terms were also highlighted, including 'SRP-dependent cotranslational protein targeting to membrane', 'protein targeting to ER', and 'translation initiation' (**Fig. 3f**). Most of these genes encoded ribosomal protein subunits that were preferentially expressed in HIV-specific CD8$^+$ T cells from the LNs of ECs (**Fig. 4e**). Gene set enrichment analysis (GSEA) similarly identified 'translation', 'SRPdependent cotranslational protein targeting to membrane', and '3' UTR-mediated translation regulation' as the most highly enriched gene sets in the EC group (**Fig. 4f**).

We then performed *in vitro* translation experiments to measure the uptake of fluorescently labeled L-homopropargylglycine (HPG) in resting and activated CD8$^+$ T cells from the LNs of ECs, CPs, and HIV$^+$ individuals on ART. Higher frequencies of resting memory CD8$^+$ T cells from the LNs of ECs incorporated HPG into newly synthesized proteins compared with resting

memory $CD8^+$ T cells from the LNs of CPs ($p = 0.003$) (**Fig. 4g**). These differences emanated primarily from the central memory compartment (**Fig. 4g**). After stimulation with HIV-derived peptides or anti-CD3, functionally responsive $CD8^+$ T cells from the LNs of ECs also incorporated more HPG than functionally responsive $CD8^+$ T cells from the LNs of CPs ($p = 0.008$ and $p = 0.01$, respectively) and functionally responsive $CD8^+$ T cells from the LNs of HIV^+ individuals on ART ($p = 0.004$ and $p = 0.04$, respectively) (**Fig. 4g**). These results suggest that efficient protein translation can explain, at least in part, the antiviral efficacy and polyfunctional nature of HIV-specific $CD8^+$ T cells in ECs.

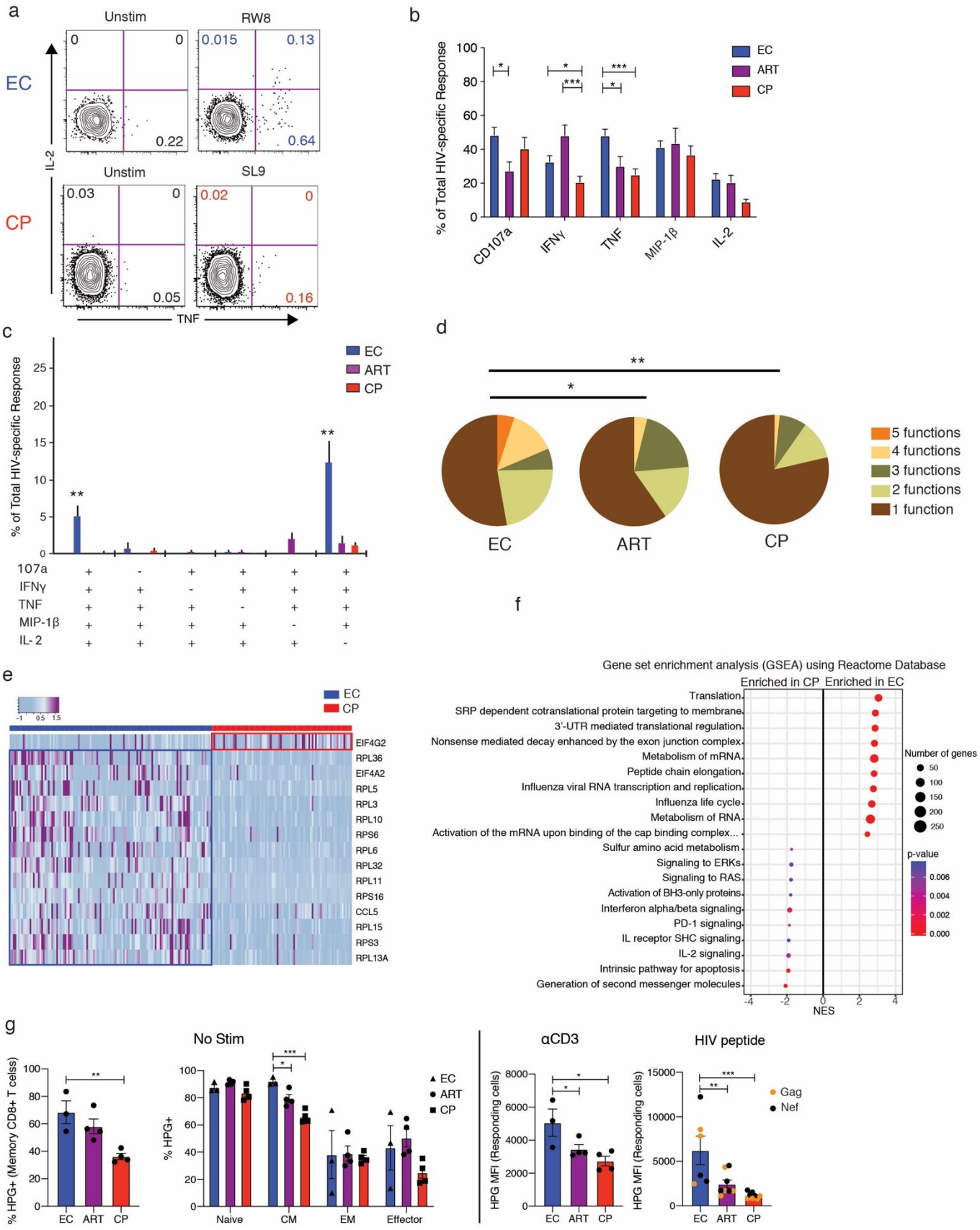
a
Unstim
RW8
EC
CP
IL-2
TNF
0
0.22
0.015
0.13
0.64
0.03
0.05
0.02
0.16
SL9
b
% of Total HIV-specific Response
EC
ART
CP
CD107a
IFNγ
TNF
MIP-1β
IL-2
c
% of Total HIV-specific Response
107a
IFNγ
TNF
MIP-1β
IL-2
d
5 functions
4 functions
3 functions
2 functions
1 function
e
EIF4G2
RPL36
EIF4A2
RPL5
RPL3
RPL10
RPS6
RPL6
RPL32
RPL11
RPS16
CCL5
RPL15
RPS3
RPL13A
f
Gene set enrichment analysis (GSEA) using Reactome Database
Enriched in CP
Enriched in EC
Translation
SRP dependent cotranslational protein targeting to membrane
3'-UTR mediated translational regulation
Nonsense mediated decay enhanced by the exon junction complex
Metabolism of mRNA
Peptide chain elongation
Influenza viral RNA transcription and replication
Influenza life cycle
Metabolism of RNA
Activation of the mRNA upon binding of the cap binding complex...
Sulfur amino acid metabolism
Signaling to ERKs
Signaling to RAS
Activation of BH3-only proteins
Interferon alpha/beta signaling
PD-1 signaling
IL receptor SHC signaling
IL-2 signaling
Intrinsic pathway for apoptosis
Generation of second messenger molecules
Number of genes
p-value
NES
g
No Stim
αCD3
HIV peptide
% HPG+ (Memory CD8+ T celss)
% HPG+
HPG MFI (Responding cells)
Naive
CM
EM
Effector
Gag
Nef

DISCUSSION

In this study, we found that weakly cytolytic $CD8^+$ T cells homed to B cell follicles, which constitute a major viral reservoir *in vivo (2, 15)*, and potently suppressed HIV replication in the LTs of ECs. Moreover, these LN-derived $CD8^+$ T cells downregulated inhibitory receptors, upregulated multiple soluble factors and cytokines, and displayed efficient protein translation. Although cause and effect arguments can always be made in the context of human studies, these features likely identify a protective immune signature, because $CD8^+$ T cells from the LNs of HIV^+ individuals on ART failed to acquire the characteristics of $CD8^+$ T cells from the LNs of ECs.

Ultrasensitive assays have revealed ongoing viral replication and evolution in the plasma of ECs *(23-25)*. In line with the notion of anatomically localized immune control, we detected very few $vRNA^+$ cells and very low amounts of HIV DNA and RNA in the LNs of ECs. We also found that $CD8^+$ T cells from the LNs of ECs suppressed HIV replication in autologous $CD4^+$ T cells far more efficiently than $CD8^+$ T cells from the LNs of CPs and $CD8^+$ T cells from the LNs of HIV^+ individuals on ART. Depletion studies in non-human primates have shown that $CD8^+$ cells are required to maintain effective control of SIV *(2, 50)*. Moreover, we and others have demonstrated that circulating $CD8^+$ T cells exhibit superior cytolytic activity in ECs *(6, 7)*. It was therefore surprising to find that cytolytic molecules were expressed at lower levels in $CD8^+$ T cells from the LNs of ECs compared with $CD8^+$ T cells from the LNs of CPs, aligning with a general state of limited immunosurveillance in HIV-infected LTs *(42)*. Although we cannot exclude a role for cytolytic mechanisms, especially during the early stages of infection, our data clearly show that a potent cytolytic response is not a prerequisite for durable immune-mediated

suppression of HIV. These data are consistent with the observation that terminally differentiated effector memory T cells, which are highly cytolytic, primarily circulate in the blood and patrol highly vascularized organs rather than other tissue sites *(51)*. The general exclusion of cytolytic $CD4^+$ and $CD8^+$ T cells from LTs is likely a conserved feature of the immune system that has evolved to limit the destruction of antigen-presenting cells and stromal tissues under conditions of persistent stimulation. Non-cytolytic effector functions may therefore be necessary for effective immune control of viruses and other pathogens that specifically target these sites. Indeed, an equivalent scenario has been described in the liver, where hepatitis B virus-specific $CD8^+$ T cells eliminate the infection without killing hepatocytes via the secretion of IFNγ and TNF *(52)*. Similarly, non-cytolytic mechanisms of immune control have been described in the context of infection with herpes simplex virus, measles virus, and vaccinia virus *(53, 54)*, as well as HIV and SIV infection *(55-57)*. Our results adds to this body of literature and further suggest that spatial distribution and the efficient translation of antiviral proteins are key features of a protective HIV-specific $CD8^+$ T cell response in LTs.

In summary, we have shown that non-cytolytic $CD8^+$ T cells with distinct functional, phenotypic, and transcriptional signatures, including the upregulation of known or predicted soluble factors, efficient protein translation, and a high level of ribosome biogenesis, suppress viral replication in the LNs of ECs. These observations are highly pertinent in light of current "kill" strategies designed to achieve a functional cure for HIV *(58)*. Collectively, our data support a model in which viral suppression rather than viral eradication dictates immune efficacy, without excluding a role for cytolytic mechanisms, and provide fresh impetus in the search for novel antiviral factors that may complement existing therapies for HIV *(59)*.

MATERIALS AND METHODS

Samples

Peripheral blood samples, tissue biopsies (cervical, iliac, or inguinal LNs), and fine needle aspirates (inguinal LNs) were obtained from HIV^+ individuals on ART (n = 10) and untreated HIV^+ individuals categorized as acute seroconverters (Fiebig stage IV–VI, n = 7), ECs (n = 12), or CPs (n = 13). Donors were recruited at three different sites: INER-CIENI, Mexico City, Mexico; the University of California, San Francisco, USA; and the University of Pennsylvania, Philadelphia, USA. Clinical characteristics are summarized in **Supplementary Table 1**. Paraffin-embedded LN slides from CPs (n = 7) for microscopy experiments were obtained via the Pathology Core at the Hospital of the University of Pennsylvania (Philadelphia). All donors provided informed consent in line with protocols approved by the INER-CIENI Ethics Committee, the Federal Commission for the Protection against Sanitary Risk (COFEPRIS), and the Institutional Review Boards of the University of California (San Francisco) and the University of Pennsylvania (Philadelphia). Sample sizes were not predetermined by power calculations, and investigators were not blinded to group identity during the course of the study.

Peripheral blood mononuclear cells (PBMCs) were isolated using standard density gradient centrifugation, and LN mononuclear cells (LNMCs) were collected from whole biopsies via mechanical homogenization. Fine needle aspirates were processed for immediate experimentation. PBMCs and LNMCs were cryopreserved at –140 °C.

RNAscope

Next-generation *in situ* hybridization was performed on LN biopsies as described previously *(60)*.

qPCR quantification of cellular HIV-1 DNA and RNA

Cell-associated DNA and RNA were purified using an AllPrep DNA/RNA Mini Kit (Qiagen), concentrated in a SpeedVac System (Thermo Fisher Scientific), and normalized to cell equivalents via quantitative PCR (qPCR) with reference to genomic telomerase reverse transcriptase for DNA and expressed ribosomal protein lateral stalk subunit P0 for RNA (Thermo Fisher Scientific). Total cell-associated HIV DNA and RNA were quantified via qPCR using a QuantStudio 6 Flex RealTime PCR System (Applied Biosystems) with the LTR-specific primers F522-43 (5'-GCCTCAATAAAGCTTGCCTTGA-3'; HXB2 522–543) and R626-43 (5'-GGGCGCCACTGCTAGAGA-3'; HXB2 626–643) and a FAM-BQ probe (5'CCAGAGTCACACAACAGACGGGCACA-3'). Cell-associated HIV DNA copy number was determined in a final reaction volume of 20 μL incorporating 4 pmol of each primer, 4 pmol of probe, 5 μL of DNA, and 10 μL of 2x TaqMan Universal Master Mix II, with UNG (Thermo Fisher Scientific). Thermal parameters were as follows: 50 °C for 2 minutes (1 cycle), 95 °C for 10 minutes (1 cycle), and 95 °C for 15 seconds followed by 59 °C for 1 minute (60 cycles). Cell-associated HIV RNA copy number was determined in a final reaction volume of 20 μL incorporating 4 pmol of each primer, 4 pmol of probe, 5 μL of RNA, 0.5 μL of reverse transcriptase, and 10 μL of 2x TaqMan RNA-to-CT 1-Step (Thermo Fisher Scientific). Thermal parameters were as follows: 48 °C for 20 minutes (1 cycle), 95 °C for 10 minutes (1 cycle), and 95 °C for 15 seconds followed by 59 °C for 1 minute (60 cycles). For HIV DNA measurements, external quantification standards were prepared from the ACH-2 cell line in a background of HIV^- human cellular DNA, calibrated against the Division of AIDS Virology Quality Assurance

Program HIV-1 DNA Quantification Standard (National Institutes of Health AIDS Reagent Program). For HIV RNA measurements, external quantification standards were prepared from full-length NL4-3 virion RNA, and copy number was determined using a Real-Time HIV-1 Viral Load Assay (Abbott Molecular), calibrated against the Division of AIDS Virology Quality Assurance Program HIV-1 RNA Quantification Standard (National Institutes of Health AIDS Reagent Program). Copy number for all samples was determined in triplicate by extrapolation against a seven-point standard curve (1–10,000 cps).

Peptide stimulation assay

Cryopreserved LNMCs and PBMCs were thawed and rested overnight at 37 °C in RPMI medium supplemented with 10% fetal bovine serum, 1% L-glutamine, and 1% penicillin/streptomycin (R10). Cells were then washed in R10 and resuspended at 2 x 10^6 cells/mL. Approximately 0.5 x 10^6 to 1 x 10^6 cells were used per condition, with lower bounds defined by cell availability in each sample. All stimulation conditions included anti-CD28 and anti-CD49d (each at 1 μg/mL, BD Biosciences), GolgiStop (0.7 μL/mL, BD Biosciences), and brefeldin A (1 μg/mL, Sigma-Aldrich). Cells were stimulated for 6 hours at 37 °C with peptides matching optimal epitopes derived from HIV (each at a final concentration of 1 μg/mL, New England Biolabs). Positive controls incorporated staphylococcal enterotoxin B (1 μg/mL, Sigma-Aldrich). Degranulation was detected via the addition of anti-CD107a–PE-Cy5 (eBioH4A3, eBioscience) at the start of the assay to capture surface-mobilized events in real time *(61)*.

Flow cytometry

LNMCs and PBMCs were stained with anti-CCR7–APC-Cy7 (G043H7, BioLegend) for 10 minutes at 37 °C. Cells were then labeled with LIVE/DEAD Fixable Aqua (Thermo Fisher Scientific) for 10 minutes at room temperature to identify non-viable events, stained with a cocktail of directly-conjugated monoclonal antibodies for 20 minutes at room temperature to detect surface markers, fixed/permeabilized using a Cytofix/Cytoperm Kit (BD Biosciences), stained with another cocktail of directly-conjugated monoclonal antibodies for 1 hour at room temperature to detect intracellular markers, and fixed in 1% paraformaldehyde (Sigma-Aldrich). Data were acquired using an LSRII flow cytometer (BD Biosciences) and analyzed with FlowJo software v9.9.4 (Tree Star Inc.).

Antibodies

The following directly-conjugated reagents were used in flow cytometry experiments. Tetramer panel: anti-CCR7–APC-Cy7 (G043H7, BioLegend), anti-CD14–BV510 (M5E2, BioLegend), anti-CD19–BV510 (HIB19, BioLegend), anti-CD3–BV711 (UCHT1, BioLegend), anti-CD4–PE-Cy5.5 (S3.5, Thermo Fisher Scientific), anti-CD8–BV570 (RPA-T8, BioLegend), anti-CD27–BV785 (O323, BioLegend), anti-CD45RO–BV650 (UCHL1, BioLegend), anti-CD69–PE-Cy5 (TP1.55.3, Beckman Coulter), anti-CD103–BV605 (2E7, BioLegend), anti-CXCR5–AF488 (RF8B2, BD Biosciences), anti-perforin–PE-Cy7 (dG9, eBioscience), anti-granzyme B–AF700 (GB11, BD Biosciences), anti-Tbet–PE-Dazzle (4B10, BioLegend), and anti-Eomes–AF647 (WD1928, eBioscience). Peptide stimulation panel: anti-CD107a–PE-Cy5 (eBioH4A3, eBioscience), anti-CCR7–APC-Cy7 (G043H7, BioLegend), anti-CD14–BV510 (M5E2, BioLegend), anti-CD19–BV510 (HIB19, BioLegend), anti-CD3–BV711 (UCHT1, BioLegend), anti-CD4–PE-Cy5.5 (S3.5, Thermo Fisher Scientific), anti-CD8–BV570 (RPA-T8, BioLegend),

anti-CD27–BV785 (O323, BioLegend), anti-CD45RO–BV650 (UCHL1, BioLegend), anti-CXCR5–AF647 (RF8B2, BD Biosciences), anti-IFNγ–FITC (B27, BD Biosciences), anti-TNF–BV605 (MAb11, BioLegend), anti-IL-2–APC-R700 (MQ1-17H12, BD Biosciences), anti-MIP-1β–PE-Cy7 (D21-1351, BD Biosciences), anti-perforin–BV421 (B-D48, BioLegend), anti-granzyme B–PE-TxRed (GB11, Thermo Fisher Scientific), and anti-Tbet–PE (4B10, eBioscience). Redirected killing assay panel: anti-active caspase 3–FITC (C92-605, BD Biosciences), anti-CD3–PE (SK7, BD Biosciences), and anti-perforin–PE-Cy7 (dG9, eBioscience). Suppression assay panel: anti-p24–FITC (KC57, Beckman Coulter), anti-CD14–BV510 (M5E2, BioLegend), anti-CD19–BV510 (HIB19, BioLegend), anti-CD3–BV711 (UCHT1, BioLegend), anti-CD4–PE-Cy7 (RPA-T4, BioLegend), anti-CD8–BV570 (RPA-T8, BioLegend), anti-CD25–Tricolor (CD25-3G10, Thermo Fisher Scientific), anti-perforin–BV421 (B-D48, BioLegend), and anti-granzyme B–PE-TxRed (GB11, Thermo Fisher Scientific). Translation assay panel: anti-CCR7–APC-Cy7 (G043H7, BioLegend), anti-CD14–BV510 (M5E2, BioLegend), anti-CD19–BV510 (HIB19, BioLegend), anti-CD3–BV711 (UCHT1, BioLegend), anti-CD4–APC (S3.5, Thermo Fisher Scientific), anti-CD8–BV570 (RPA-T8, BioLegend), anti-CD45RO–BV650 (UCHL1, BioLegend), azide–AF488 (A10266, Thermo Fisher Scientific), anti-TNF–PE-Cy7 (MAb11, Thermo Fisher Scientific), and anti-IFNγ–AF700 (B27, BD Biosciences). Viral quantification panel: anti-CCR7–APC-Cy7 (G043H7, BioLegend), anti-CD3–APC-R700 (UCHT1, BD Biosciences), anti-CD4–PE-Cy7 (RPA-T4, BioLegend), anti-CD8–PE-Cy5.5 (RPA-T8, eBiosciences), anti-CD14–BV510 (M5E2, BioLegend), anti-CD19–BV510 (HIB19, BioLegend), anti-CD45RA–PE-CF594 (HI100, BD Biosciences), anti-CXCR5–AF647 (RF8B2, BD Biosciences), and anti-PD-1–BV421 (EH12.2H7, BioLegend).

Tetramers

HLA class I tetramers conjugated to BV421 or PE were produced as described previously *(62)*. The following specificities were used to detect HIV-specific $CD8^+$ T cells: A*0201-IV9 (ILKEPVHGV), A*0201-SL9 (SLYNTVATL), A*0201-FK10 (FLGKIWPSHK), A*0201-TV9 (TLNAWVKVV), A*2402-RW8 (RYPLTFGW), A*2402-KW9 (KYKLKHIVW), A*2402-RL9 (RPMTYKGAL), B*0702-GL9 (GPGHKARVL), B*0702-HI10 (HPRVSSEVHI), B*0702-SM9 (SPAIFQSSF), B*2705-KK10 (KRWIILGLNK), B*3501-VY10 (VPLDEDFRKY), B*3501NY9 (NSSKVSQNY), B*5701-KF11 (KAFSPEVIPMF), B*5701-TW10 (TSTLQEQIGW), B*5701-ISW9 (ISPRTLNAW), and B*5701-QW9 (QASQEVKNW).

Immunohistochemistry

LN biopsy material was cut at a thickness of 5 μm and processed as described previously *(63)*. Briefly, tissue sections were heated in 0.01% citraconic anhydride containing 0.05% Tween-20 and incubated overnight at 4 ^oC with monoclonal or polyclonal antibodies specific for perforin (1:100, 5B10/VP-P967, Vector Laboratories Inc.) or granzyme B (1:200, HPA003418, Sigma-Aldrich). Slides were then washed in TBS containing 0.05% Tween-20, and endogenous peroxidases were blocked using 1.5% (v/v) H_2O_2 in TBS, pH 7.4. Antigens were revealed using mouse Polink-1 or rabbit Polink-2 HRP in conjunction with ImmPACT DAB (Vector Laboratories Inc.) and Warp Red (Biocare Medical Inc.). Slides were then washed in H_2O, counterstained with haematoxylin, mounted in Permount (Thermo Fisher Scientific), and scanned at 200x magnification using a ScanScope CS System (Aperio Technologies). Representative regions of interest (0.4 mm^2) were identified visually, and high-resolution images were extracted

from the whole-tissue scans. The percent area positive for $CD4^+$ T cells was quantified using CellProfiler v3.1.5 *(64)*.

Single-cell RNAseq

The experimental setup was described previously in Buggert *et al. (22)*. Briefly, single HIV $tetramer^+$ cells were index sorted directly into 96-well microtiter plates containing lysis buffer using a FACSAria II flow cytometer (BD Biosciences). Cellular nucleic acids were recovered using an RNEasy Plus Micro Kit (Qiagen) and RNAClean (SPRI) beads (Beckman Coulter). Performance was assessed using External RNA Controls Consortium (ERCC) RNA Spike-In Mix (Ambion). Reverse transcription was performed using oligo-dT primers, and cDNA was amplified over 22–24 PCR cycles using universal primers and Kapa HiFi HotStart ReadyMix (Kapa Biosystems). After clean-up, amplified cDNA was barcoded using Illumina Nextera libraries and sequenced to a depth of approximately 2 million 150 bp paired-end reads/cell on a HiSeq 4000 (Illumina). Whole transcriptome data were obtained from 221 cells (n = 552 sorted cells).

Single-cell RNAseq analyses

A kernel-method learning framework was used to assess the pairwise similarity between cells and compute the distance metric that best fitted the structure of the data (https://arxiv.org/pdf/1808.02061.pdf). Cell-to-cell similarity was learned using a rank-based, nonparametric function, and tSNE kernelization allowed the use of data from all available features. Dimensionality reduction was performed using kernel tSNE, wherein the pairwise similarity between cells was computed using the Semblance kernel as a distance measure. In determination of the cell-to-cell similarity matrix, the Gini index was used to account for the

distribution of each gene and weigh it appropriately in the kernel calculation. The Gini index enabled the prioritization of genes with high variance as the genes that were more likely to provide useful features for niche group detection. Single cells were then projected onto a two-dimensional space using kernel tSNE, enabling intuitive visualization of hidden structures within the data. The supporting code is freely available online and can be implemented via the R Package Semblance (https://cran.rproject.org/web/packages/Semblance/index.html).

For support vector machine (SVM) analyses, genes were selected using a t-score cut-off of $p < 0.01$. Selected genes were then ranked using L0-norm regularization. The L0-norm-ranked gene lists were fed into the SVM algorithm for cross-validation (k-fold = 10) in subsets (increment = 100 genes). The average prediction error for each cross-validation was used to determine how well each subset of genes classified the desired labels. All steps were performed in MATLAB (MathWorks). L0-norm regularization was implemented using the MATLAB Feature Selection Library (MathWorks).

Differentially expressed genes were identified using three approaches: ROTS *(40)*, which optimizes the t-statistics based on the inherent characteristics of the data; scDD *(41)* which is a differential expression analysis method that accounts for the possibility of multimodally distributed gene expression; and Seurat *(42)*, which uses the non-parametric Mann-Whitney U-test to assess the null hypothesis that a randomly selected mean expression value for a given gene in one group will have an equal chance of being less than or greater than a randomly selected mean expression value for the same gene in a second group. As different genes in the dataset exhibited different distribution properties, these approaches in combination allowed us to

winnow the list of differentially expressed genes, specifying a cut-off of $p < 0.05$ in at least two of the three outputs. The scDD p-values are reported for simplicity.

The topGO package Bioconductor v3.8 was used for GO analyses (https://bioconductor.org/packages/release/bioc/html/topGO.html). GO terms associated with each gene were obtained using the August 2017 ENSEMBL Database. Significance was determined using the classic Fisher method. GSEA analyses were performed using software developed by the Broad Institute *(65, 66)*.

Redirected killing assay

P815 mastocytoma target cells were labeled with LIVE/DEAD Violet (Thermo Fisher Scientific) and TFL4 (OncoImmun), washed twice in PBS, and incubated for 30 minutes at room temperature with anti-CD3 (5µg/mL, UCHT1, BioRad). $CD8^+$ T cells were negatively selected from LNMCs or PBMCs using a $CD8^+$ T Cell Enrichment Kit (StemCell Technologies). Isolated $CD8^+$ T cells were rested in R10 for at least 45 minutes at 37 °C and then incubated with anti-CD3-coated P815 cells at different effector-to-target ratios in a 96-well V-bottom plate for 4 hours at 37 °C. Cells were then stained as described above (see Antibodies section) and acquired using an LSRII flow cytometer (BD Biosciences).

Killing capacity was calculated by subtracting the frequency of active $caspase3^+$ $TFL4^+$ $LIVE/DEAD^-$ P815 cells in target-only wells from the frequency of active $caspase3^+$ $TFL4^+$ $LIVE/DEAD^-$ P815 cells in wells containing effector cells.

Viral suppression assay

The viral suppression assay was modified from Sáez-Cirion *et al. (27)*. Briefly, $CD4^+$ T cells were positively selected from LNMCs or PBMCs using a $CD4^+$ T Cell Enrichment Kit (StemCell Technologies) and activated using a cocktail of IL-2 (100 U/mL, Chiron), anti-CD3 (1 μg/mL, UCHT1, Bio-Rad), anti-CD28 (1 μg/mL, L293, BD Biosciences), and anti-CD49d (1 μg/mL, L25, BD Biosciences). Concurrently, autologous $CD8^+$ T cells were negatively selected from LNMCs or PBMCs using a $CD8^+$ T Cell Enrichment Kit (StemCell Technologies) and rested in R10. After 2 days, $CD4^+$ T cells were infected with HIV-1 BAL by spinoculation and incubated with or without autologous $CD8^+$ T cells in the absence of exogenous IL-2. Cells were harvested after a further 3 days, stained as described above (see Antibodies section), and acquired using an LSRII flow cytometer (BD Biosciences).

Suppression capacity was calculated by dividing the frequency of $p24^+$ $CD4^+$ T cells in wells containing autologous $CD8^+$ T cells by the frequency of $p24^+$ $CD4^+$ T cells in wells lacking autologous $CD8^+$ T cells.

HPG translation assay

The protein translation assay was adapted from Araki *et al. (67)*. Briefly, LNMCs were rested overnight and incubated for 30 minutes in methionine-free R10. The cultures were then supplemented with Click-iT HPG (100 μM, Thermo Fisher Scientific). Cells were stimulated with PepMix HIV (GAG) Ultra (2μg/mL/peptide, JPT Peptide Technologies), PepMix HIV (NEF) Ultra (2μg/mL/peptide, JPT Peptide Technologies), or anti-CD3 (5μg/mL, UCHT1,

BioRad) in the presence of GolgiStop (0.7 μL/mL, BD Biosciences) and brefeldin A (1 μg/mL, Sigma-Aldrich). After 6 hours, cells were stained as described above (see Antibodies section) and acquired using an LSRII flow cytometer (BD Biosciences), following the instructions in the Click-iT Plus Alexa Fluor Picolyl Azide Toolkit (Thermo Fisher Scientific).

Statistics for non-sequencing data

Data were checked for normality using the Shapiro-Wilk normality test. Parametric tests were used if the data passed the normality test, and non-parametric tests were used if the data failed the normality test. Multiple corrections for two-way ANOVA were performed using the two-stage linear step-up procedure of Benjamini, Krieger, and Yekutieli. Specific tests are indicated in the relevant figure legends. Analyses were performed using R Studio or Prism v7.0 (GraphPad).

REFERENCES

1. S. G. Deeks, B. D. Walker, Human immunodeficiency virus controllers: mechanisms of durable virus control in the absence of antiretroviral therapy, *Immunity* **27**, 406–416 (2007).

2. Y. Fukazawa, R. Lum, A. A. Okoye, H. Park, K. Matsuda, J. Y. Bae, S. I. Hagen, R. Shoemaker, C. Deleage, C. Lucero, D. Morcock, T. Swanson, A. W. Legasse, M. K. Axthelm, J. Hesselgesser, R. Geleziunas, V. M. Hirsch, P. T. Edlefsen, M. Piatak, J. D. Estes, J. D. Lifson, L. J. Picker, B cell follicle sanctuary permits persistent productive simian immunodeficiency virus infection in elite controllers, *Nat. Med.* **21**, 132–139 (2015).

3. M. R. Betts, M. C. Nason, S. M. West, S. C. De Rosa, S. A. Migueles, J. Abraham, M. M. Lederman, J. M. Benito, P. A. Goepfert, M. Connors, M. Roederer, R. A. Koup, HIV

nonprogressors preferentially maintain highly functional HIV-specific $CD8^+$ T cells, *Blood* **107**, 4781–4789 (2006).

4. J. R. Almeida, D. A. Price, L. Papagno, Z. A. Arkoub, D. Sauce, E. Bornstein, T. E. Asher, A. Samri, A. Schnuriger, I. Theodorou, D. Costagliola, C. Rouzioux, H. Agut, A.-G. Marcelin, D. Douek, B. Autran, V. Appay, Superior control of HIV-1 replication by $CD8^+$ T cells is reflected by their avidity, polyfunctionality, and clonal turnover, *J. Exp. Med.* **204**, 2473–2485 (2007).

5. S. A. Migueles, A. C. Laborico, W. L. Shupert, M. S. Sabbaghian, R. Rabin, C. W. Hallahan, D. van Baarle, S. Kostense, F. Miedema, M. McLaughlin, L. Ehler, J. Metcalf, S. Liu, M. Connors, HIV-specific $CD8^+$ T cell proliferation is coupled to perforin expression and is maintained in nonprogressors, *Nat. Immunol.* **3**, 1061–1068 (2002).

6. S. A. Migueles, C. M. Osborne, C. Royce, A. A. Compton, R. P. Joshi, K. A. Weeks, J. E. Rood, A. M. Berkley, J. B. Sacha, N. A. Cogliano-Shutta, M. Lloyd, G. Roby, R. Kwan, M. McLaughlin, S. Stallings, C. Rehm, M. A. O'Shea, J. Mican, B. Z. Packard, A. Komoriya, S. Palmer, A. P. Wiegand, F. Maldarelli, J. M. Coffin, J. W. Mellors, C. W. Hallahan, D. A. Follman, M. Connors, Lytic granule loading of $CD8^+$ T cells is required for HIV-infected cell elimination associated with immune control, *Immunity* **29**, 1009–1021 (2008).

7. A. R. Hersperger, F. Pereyra, M. Nason, K. Demers, P. Sheth, L. Y. Shin, C. M. Kovacs, B. Rodriguez, S. F. Sieg, L. Teixeira-Johnson, D. Gudonis, P. A. Goepfert, M. M. Lederman, I. Frank, G. Makedonas, R. Kaul, B. D. Walker, M. R. Betts, Perforin expression directly ex vivo by HIV-specific CD8 T-cells is a correlate of HIV elite control, *PLoS Pathog.* **6**, e1000917 (2010).

8. L. R. McKinnon, R. Kaul, J. Kimani, N. J. Nagelkerke, C. Wachihi, K. R. Fowke, T. B. Ball, F. A. Plummer, HIV-specific $CD8^+$ T-cell proliferation is prospectively associated with delayed disease progression, *Immunol. Cell Biol.* **90**, 346–351 (2012).

9. M. M. Addo, R. Draenert, A. Rathod, C. L. Verrill, B. T. Davis, R. T. Gandhi, G. K. Robbins, N. O. Basgoz, D. R. Stone, D. E. Cohen, M. N. Johnston, T. Flynn, A. G. Wurcel, E. S. Rosenberg, M. Altfeld, B. D. Walker, Fully differentiated HIV-1 specific $CD8^+$ T effector cells are more frequently detectable in controlled than in progressive HIV-1 infection, *PLoS ONE* **2**, e321 (2007).

10. P. J. Goulder, R. E. Phillips, R. A. Colbert, S. McAdam, G. Ogg, M. A. Nowak, P. Giangrande, G. Luzzi, B. Morgan, A. Edwards, A. J. McMichael, S. Rowland-Jones, Late escape from an immunodominant cytotoxic T-lymphocyte response associated with progression to AIDS, *Nat. Med.* **3**, 212–217 (1997).

11. S. A. Migueles, M. S. Sabbaghian, W. L. Shupert, M. P. Bettinotti, F. M. Marincola, L. Martino, C. W. Hallahan, S. M. Selig, D. Schwartz, J. Sullivan, M. Connors, HLA B*5701 is highly associated with restriction of virus replication in a subgroup of HIV-infected long term nonprogressors, *Proc. Natl. Acad. Sci. U. S. A.* **97**, 2709–2714 (2000).

12. G. Pantaleo, C. Graziosi, L. Butini, P. A. Pizzo, S. M. Schnittman, D. P. Kotler, A. S. Fauci, Lymphoid organs function as major reservoirs for human immunodeficiency virus, *Proc. Natl. Acad. Sci. U. S. A.* **88**, 9838–9842 (1991).

13. G. Pantaleo, C. Graziosi, J. F. Demarest, L. Butini, M. Montroni, C. H. Fox, J. M. Orenstein, D. P. Kotler, A. S. Fauci, HIV infection is active and progressive in lymphoid tissue during the clinically latent stage of disease, *Nature* **362**, 355–358 (1993).

14. G. Pantaleo, C. Graziosi, J. F. Demarest, O. J. Cohen, M. Vaccarezza, K. Gantt, C. Muro Cacho, A. S. Fauci, Role of lymphoid organs in the pathogenesis of human immunodeficiency virus (HIV) infection, *Immunol. Rev.* **140**, 105–130 (1994).

15. M. Perreau, A.-L. Savoye, E. De Crignis, J.-M. Corpataux, R. Cubas, E. K. Haddad, L. De Leval, C. Graziosi, G. Pantaleo, Follicular helper T cells serve as the major CD4 T cell compartment for HIV-1 infection, replication, and production, *J. Exp. Med.* **210**, 143–156 (2013).

16. J. D. Estes, C. Kityo, F. Ssali, L. Swainson, K. N. Makamdop, G. Q. Del Prete, S. G. Deeks, P. A. Luciw, J. G. Chipman, G. J. Beilman, T. Hoskuldsson, A. Khoruts, J. Anderson, C. Deleage, J. Jasurda, T. E. Schmidt, M. Hafertepe, S. P. Callisto, H. Pearson, T. Reimann, J. Schuster, J. Schoephoerster, P. Southern, K. Perkey, L. Shang, S. W. Wietgrefe, C. V. Fletcher, J. D. Lifson, D. C. Douek, J. M. McCune, A. T. Haase, T. W. Schacker, Defining total-body AIDS-virus burden with implications for curative strategies, *Nat. Med.* **23**, 1271–1276 (2017).

17. J. Andersson, H. Behbahani, J. Lieberman, E. Connick, A. Landay, B. Patterson, A. Sönnerborg, K. Loré, S. Uccini, T. E. Fehniger, Perforin is not co-expressed with granzyme A within cytotoxic granules in CD8 T lymphocytes present in lymphoid tissue during chronic HIV infection, *AIDS* **13**, 1295–1303 (1999).

18. M. A. Reuter, P. M. Del Río Estrada, M. Buggert, C. Petrovas, S. Ferrando-Martinez, S.

Nguyen, A. Sada Japp, Y. Ablanedo-Terrazas, A. Rivero-Arrieta, L. Kuri-Cervantes, H. M. Gunzelman, E. Gostick, D. A. Price, R. A. Koup, A. Naji, D. H. Canaday, G. Reyes-Terán, M. R. Betts, HIV-specific $CD8^+$ T cells exhibit reduced and differentially regulated cytolytic activity in lymphoid tissue, *Cell Rep.* **21**, 3458–3470 (2017).

19. M. Buggert, S. Nguyen, L. M. McLane, M. Steblyanko, N. Anikeeva, D. Paquin-Proulx, P. M. Del Río Estrada, Y. Ablanedo-Terrazas, K. Noyan, M. A. Reuter, K. Demers, J. K. Sandberg, M. A. Eller, H. Streeck, M. Jansson, P. Nowak, A. Sönnerborg, D. H. Canaday, A. Naji, E. J. Wherry, M. L. Robb, S. G. Deeks, G. Reyes-Terán, Y. Sykulev, A. C. Karlsson, M. R. Betts, Limited immune surveillance in lymphoid tissue by cytolytic $CD4^+$ T cells during health and HIV disease, *PLoS Pathog.* **14**, e1006973 (2018).

20. H. G. Woon, A. Braun, J. Li, C. Smith, J. Edwards, F. Sierro, C. G. Feng, R. Khanna, M. Elliot, A. Bell, A. D. Hislop, S. G. Tangye, A. B. Rickinson, T. Gebhardt, W. J. Britton, U. Palendira, Compartmentalization of total and virus-specific tissue-resident memory $CD8^+$ T cells in human lymphoid organs, *PLoS Pathog.* **12**, e1005799 (2016).

21. B. V. Kumar, W. Ma, M. Miron, T. Granot, R. S. Guyer, D. J. Carpenter, T. Senda, X. Sun, S.-H. Ho, H. Lerner, A. L. Friedman, Y. Shen, D. L. Farber, Human tissue-resident memory T cells are defined by core transcriptional and functional signatures in lymphoid and mucosal sites, *Cell Rep.* **20**, 2921–2934 (2017).

22. M. Buggert, S. Nguyen, G. Salgado-Montes de Oca, B. Bengsch, S. Darko, A. Ransier, E. R. Roberts, D. Del Alcazar, I. B. Brody, L. A. Vella, L. Beura, S. Wijeyesinghe, R. S. Herati, P. M. Del Río Estrada, Y. Ablanedo-Terrazas, L. Kuri-Cervantes, A. Sada Japp, S. Manne, S.

Vartanian, A. Huffman, J. K. Sandberg, E. Gostick, G. Nadolski, G. Silvestri, D. H. Canaday, D. A. Price, C. Petrovas, L. F. Su, G. Vahedi, Y. Dori, I. Frank, M. G. Itkin, E. J. Wherry, S. G. Deeks, A. Naji, G. Reyes-Terán, D. Masopust, D. C. Douek, M. R. Betts, Identification and characterization of HIV-specific resident memory $CD8^+$ T cells in human lymphoid tissue, *Sci. Immunol.* **3**, eaar4526 (2018).

23. H. Mens, M. Kearney, A. Wiegand, W. Shao, K. Schonning, J. Gerstoft, N. Obel, F. Maldarelli, J. W. Mellors, T. Benfield, J. M. Coffin, HIV-1 continues to replicate and evolve in patients with natural control of HIV infection, *J. Virol.* **84**, 12971–12981 (2010).

24. K. A. O'Connell, T. P. Brennan, J. R. Bailey, S. C. Ray, R. F. Siliciano, J. N. Blankson, Control of HIV-1 in elite suppressors despite ongoing replication and evolution in plasma virus, *J. Virol.* **84**, 7018–7028 (2010).

25. J. N. Blankson, J. R. Bailey, S. Thayil, H.-C. Yang, K. Lassen, J. Lai, S. K. Gandhi, J. D. Siliciano, T. M. Williams, R. F. Siliciano, Isolation and characterization of replication-competent human immunodeficiency virus type 1 from a subset of elite suppressors, *J. Virol.* **81**, 2508–2518 (2007).

26. E. A. Boritz, S. Darko, L. Swaszek, G. Wolf, D. Wells, X. Wu, A. R. Henry, F. Laboune, J. Hu, D. Ambrozak, M. S. Hughes, R. Hoh, J. P. Casazza, A. Vostal, D. Bunis, K. NganouMakamdop, J. S. Lee, S. A. Migueles, R. A. Koup, M. Connors, S. Moir, T. Schacker, F. Maldarelli, S. H. Hughes, S. G. Deeks, D. C. Douek, Multiple origins of virus persistence during natural control of HIV infection, *Cell* **166**, 1004–1015 (2016).

27. A. Sáez-Cirión, S. Y. Shin, P. Versmisse, F. Barré-Sinoussi, G. Pancino, Ex vivo T cell–based HIV suppression assay to evaluate HIV-specific $CD8^+$ T-cell responses, *Nat. Protoc.* **5**, 1033–1041 (2010).

28. J. M. Folkvord, D. M. Anderson, J. Arya, S. MaWhinney, E. Connick, Microanatomic relationships between $CD8^+$ cells and HIV-1-producing cells in human lymphoid tissue in vivo, *J. Acquir. Immune Defic. Syndr.* **32**, 469–476 (2003).

29. J. M. Folkvord, C. Armon, E. Connick, Lymphoid follicles are sites of heightened human immunodeficiency virus type 1 (HIV-1) replication and reduced antiretroviral effector mechanisms, *AIDS Res. Hum. Retroviruses* **21**, 363–370 (2005).

30. E. Connick, T. Mattila, J. M. Folkvord, R. Schlichtemeier, A. L. Meditz, M. G. Ray, M. D. McCarter, S. MaWhinney, A. Hage, C. White, P. J. Skinner, CTL fail to accumulate at sites of HIV-1 replication in lymphoid tissue, *J. Immunol.* **178**, 6975–6983 (2007).

31. E. Connick, J. M. Folkvord, K. T. Lind, E. G. Rakasz, B. Miles, N. A. Wilson, M. L. Santiago, K. Schmitt, E. B. Stephens, H. O. Kim, R. Wagstaff, S. Li, H. M. Abdelaal, N. Kemp, D. I. Watkins, S. MaWhinney, P. J. Skinner, Compartmentalization of simian immunodeficiency virus replication within secondary lymphoid tissues of rhesus macaques is linked to disease stage and inversely related to localization of virus-specific CTL, *J. Immunol.* **193**, 5613–5625 (2014).

32. S. Li, J. M. Folkvord, E. G. Rakasz, H. M. Abdelaal, R. K. Wagstaff, K. J. Kovacs, H. O. Kim, R. Sawahata, S. MaWhinney, D. Masopust, E. Connick, P. J. Skinner, Simian immunodeficiency virus-producing cells in follicles are partially suppressed by $CD8^+$ cells in vivo, *J. Virol.* **90**, 11168–11180 (2016).

33. M. A. Rahman, K. M. McKinnon, T. S. Karpova, D. A. Ball, D. J. Venzon, W. Fan, G. Kang, Q. Li, M. Robert-Guroff, Associations of simian immunodeficiency virus (SIV)-specific follicular $CD8^+$ T cells with other follicular T cells suggest complex contributions to SIV viremia control, *J. Immunol.* **200**, 2714–2726 (2018).

34. J. H. Russell, T. J. Ley, Lymphocyte-mediated cytotoxicity, *Annu. Rev. Immunol.* **20**, 323–370 (2002).

35. I. Voskoboinik, J. C. Whisstock, J. A. Trapani, Perforin and granzymes: function, dysfunction and human pathology, *Nat. Rev. Immunol.* **15**, 388–400 (2015).

36. M. Buggert, J. Tauriainen, T. Yamamoto, J. Frederiksen, M. A. Ivarsson, J. Michaëlsson, O. Lund, B. Hejdeman, M. Jansson, A. Sönnerborg, R. A. Koup, M. R. Betts, A. C. Karlsson, T-bet and Eomes are differentially linked to the exhausted phenotype of $CD8^+$ T cells in HIV infection, *PLoS Pathog.* **10**, e1004251 (2014).

37. E. J. Wherry, M. Kurachi, Molecular and cellular insights into T cell exhaustion, *Nat. Rev. Immunol.* **15**, 486–499 (2015).

38. J. Tauriainen, L. Scharf, J. Frederiksen, A. Naji, H.-G. Ljunggren, A. Sönnerborg, O. Lund, G. Reyes-Terán, F. M. Hecht, S. G. Deeks, M. R. Betts, M. Buggert, A. C. Karlsson, Perturbed $CD8^+$ T cell TIGIT/CD226/PVR axis despite early initiation of antiretroviral treatment in HIV infected individuals, *Sci. Rep.* **7**, 40354 (2017).

39. F. Carrette, C. D. Surh, IL-7 signaling and CD127 receptor regulation in the control of T cell homeostasis, *Semin. Immunol.* **24**, 209–217 (2012).

40. T. Suomi, F. Seyednasrollah, M. K. Jaakkola, T. Faux, L. L. Elo, ROTS: an R package for reproducibility-optimized statistical testing, *PLoS Comput. Biol.* **13**, e1005562 (2017).

41. K. D. Korthauer, L.-F. Chu, M. A. Newton, Y. Li, J. Thomson, R. Stewart, C. Kendziorski, A statistical approach for identifying differential distributions in single-cell RNA-seq experiments, *Genome Biol.* **17**, 222 (2016).

42. A. Butler, P. Hoffman, P. Smibert, E. Papalexi, R. Satija, Integrating single-cell transcriptomic data across different conditions, technologies, and species, *Nat. Biotechnol.* **36**, 411–420 (2018).

43. B. R. Lane, D. M. Markovitz, N. L. Woodford, R. Rochford, R. M. Strieter, M. J. Coffey, TNF-α inhibits HIV-1 replication in peripheral blood monocytes and alveolar macrophages by inducing the production of RANTES and decreasing C-C chemokine receptor 5 (CCR5) expression, *J. Immunol.* **163**, 3653–3661 (1999).

44. F. Cocchi, A. L. DeVico, A. Garzino-Demo, S. K. Arya, R. C. Gallo, P. Lusso, Identification of RANTES, MIP-1α, and MIP-1β as the major HIV-suppressive factors produced by $CD8^+$ T cells, *Science* **270**, 1811–1815 (1995).

45. V. Appay, S. L. Rowland-Jones, RANTES: a versatile and controversial chemokine, *Trends Immunol.* **22**, 83–87 (2001).

46. V. I. Bedoya, A. Boasso, A. W. Hardy, S. Rybak, G. M. Shearer, M. T. Rugeles, Ribonucleases in HIV type 1 inhibition: effect of recombinant RNases on infection of primary T cells and immune activation-induced RNase gene and protein expression, *AIDS Res. Hum. Retroviruses* **22**, 897–907 (2006).

47. W. Zapata, W. Aguilar-Jiménez, Z. Feng, A. Weinberg, A. Russo, N. Potenza, H. Estrada, M. T. Rugeles, Identification of innate immune antiretroviral factors during in vivo and in vitro exposure to HIV-1, *Microbes Infect.* **18**, 211–219 (2016).

48. K. Monteleone, P. Di Maio, G. Cacciotti, F. Falasca, M. Fraulo, M. Falciano, I. Mezzaroma, G. D'Ettorre, O. Turriziani, C. Scagnolari, Interleukin-32 isoforms: expression, interaction with interferon-regulated genes and clinical significance in chronically HIV-1-infected patients, *Med. Microbiol. Immunol.* **203**, 207–216 (2014).

49. F. Ribeiro-Dias, R. Saar Gomes, L. L. de Lima Silva, J. C. Dos Santos, L. A. B. Joosten, Interleukin 32: a novel player in the control of infectious diseases, *J. Leukoc. Biol.* **101**, 39–52 (2017).

50. E. K. Cartwright, L. Spicer, S. A. Smith, D. Lee, R. Fast, S. Paganini, B. O. Lawson, M. Nega, K. Easley, J. E. Schmitz, S. E. Bosinger, M. Paiardini, A. Chahroudi, T. H. Vanderford, J. D. Estes, J. D. Lifson, C. A. Derdeyn, G. Silvestri, $CD8^+$ lymphocytes are required for maintaining viral suppression in SIV-infected macaques treated with short-term antiretroviral therapy, *Immunity* **45**, 656–668 (2016).

51. J. J. C. Thome, N. Yudanin, Y. Ohmura, M. Kubota, B. Grinshpun, T. Sathaliyawala, T. Kato, H. Lerner, Y. Shen, D. L. Farber, Spatial map of human T cell compartmentalization and maintenance over decades of life, *Cell* **159**, 814–828 (2014).

52. L. G. Guidotti, T. Ishikawa, M. V. Hobbs, B. Matzke, R. Schreiber, F. V. Chisari, Intracellular inactivation of the hepatitis B virus by cytotoxic T lymphocytes, *Immunity* **4**, 25–36 (1996).

53. L. G. Guidotti, F. V. Chisari, To kill or to cure: options in host defense against viral infection, *Curr. Opin. Immunol.* **8**, 478–483 (1996).

54. L. G. Guidotti, F. V. Chisari, Noncytolytic control of viral infections by the innate and adaptive immune response, *Annu. Rev. Immunol.* **19**, 65–91 (2001).

55. C. M. Walker, D. J. Moody, D. P. Stites, J. A. Levy, $CD8^+$ lymphocytes can control HIV infection in vitro by suppressing virus replication, *Science* **234**, 1563–1566 (1986).

56. N. R. Klatt, E. Shudo, A. M. Ortiz, J. C. Engram, M. Paiardini, B. Lawson, M. D. Miller, J. Else, I. Pandrea, J. D. Estes, C. Apetrei, J. E. Schmitz, R. M. Ribeiro, A. S. Perelson, G. Silvestri, $CD8^+$ lymphocytes control viral replication in SIVmac239-infected rhesus macaques without decreasing the lifespan of productively infected cells, *PLoS Pathog.* **6**, e1000747 (2010).

57. J. K. Wong, M. C. Strain, R. Porrata, E. Reay, S. Sankaran-Walters, C. C. Ignacio, T. Russell, S. K. Pillai, D. J. Looney, S. Dandekar, In vivo $CD8^+$ T-cell suppression of SIV viremia is not mediated by CTL clearance of productively infected cells, *PLoS Pathog.* **6**, e1000748 (2010).

58. L. Trautmann, Kill: boosting HIV-specific immune responses, *Curr. Opin. HIV AIDS* **11**, 409– 416 (2016).

59. J. A. Levy, The search for the $CD8^+$ cell anti-HIV factor (CAF), *Trends Immunol.* **24**, 628–632 (2003).

60. C. Deleage, S. W. Wietgrefe, G. Del Prete, D. R. Morcock, X. P. Hao, M. Piatak, J. Bess, J.

L. Anderson, K. E. Perkey, C. Reilly, J. M. McCune, A. T. Haase, J. D. Lifson, T. W. Schacker, J. D. Estes, Defining HIV and SIV reservoirs in lymphoid tissues, *Pathog. Immun.* **1**, 68–106 (2016).

61. M. R. Betts, J. M. Brenchley, D. A. Price, S. C. De Rosa, D. C. Douek, M. Roederer, R. A. Koup, Sensitive and viable identification of antigen-specific $CD8^+$ T cells by a flow cytometric assay for degranulation, *J. Immunol. Methods* **281**, 65–78 (2003).

62. D. A. Price, J. M. Brenchley, L. E. Ruff, M. R. Betts, B. J. Hill, M. Roederer, R. A. Koup, S. A. Migueles, E. Gostick, L. Wooldridge, A. K. Sewell, M. Connors, D. C. Douek, Avidity for antigen shapes clonal dominance in $CD8^+$ T cell populations specific for persistent DNA viruses, *J. Exp. Med.* **202**, 1349–1361 (2005).

63. A. Schuetz, C. Deleage, I. Sereti, R. Rerknimitr, N. Phanuphak, Y. Phuang-Ngern, J. D. Estes, N. G. Sandler, S. Sukhumvittaya, M. Marovich, S. Jongrakthaitae, S. Akapirat, J. L. K. Fletscher, E. Kroon, R. Dewar, R. Trichavaroj, N. Chomchey, D. C. Douek, R. J. O Connell, V. Ngauy, M. L. Robb, P. Phanuphak, N. L. Michael, J.-L. Excler, J. H. Kim, M. S. de Souza, J. Ananworanich, RV254/SEARCH 010 and RV304/SEARCH 013 Study Groups,
Initiation of ART during early acute HIV infection preserves mucosal Th17 function and reverses HIV-related immune activation, *PLoS Pathog.* **10**, e1004543 (2014).

64. A. E. Carpenter, T. R. Jones, M. R. Lamprecht, C. Clarke, I. H. Kang, O. Friman, D. A. Guertin, J. H. Chang, R. A. Lindquist, J. Moffat, P. Golland, D. M. Sabatini, CellProfiler: image analysis software for identifying and quantifying cell phenotypes, *Genome Biol.* **7**, R100 (2006).

65. V. K. Mootha, C. M. Lindgren, K.-F. Eriksson, A. Subramanian, S. Sihag, J. Lehar, P. Puigserver, E. Carlsson, M. Ridderstråle, E. Laurila, N. Houstis, M. J. Daly, N. Patterson, J. P. Mesirov, T. R. Golub, P. Tamayo, B. Spiegelman, E. S. Lander, J. N. Hirschhorn, D. Altshuler, L. C. Groop, PGC-1α-responsive genes involved in oxidative phosphorylation are coordinately downregulated in human diabetes, *Nat. Genet.* **34**, 267–273 (2003).

66. A. Subramanian, P. Tamayo, V. K. Mootha, S. Mukherjee, B. L. Ebert, M. A. Gillette, A. Paulovich, S. L. Pomeroy, T. R. Golub, E. S. Lander, J. P. Mesirov, Gene set enrichment analysis: A knowledge-based approach for interpreting genome-wide expression profiles, *Proc. Natl. Acad. Sci. U. S. A.* **102**, 15545–15550 (2005).

67. K. Araki, M. Morita, A. G. Bederman, B. T. Konieczny, H. T. Kissick, N. Sonenberg, R. Ahmed, Translation is actively regulated during the differentiation of $CD8^+$ effector T cells, *Nat. Immunol.* **18**, 1046–1057 (2017).

FIGURE LEGENDS

Figure 1. $CD8^+$ T cells from the LNs of ECs display superior antiviral efficacy. **a**, Representative RNAscope images of paraffin-embedded LN biopsies from one EC and one CP (left) and data quantification across donor groups (right). TCZ, T cell zone; BCF, B cell follicle. **b**, Quantification of cell-associated HIV DNA and RNA from negatively-selected $CD4^+$ T cells by qPCR. One data point on the DNA plot was adjusted from 0 to 1 for graphical purposes. Error bars represent mean and SEM. **c**, Representative flow plots from a viral suppression assay using LN-derived $CD8^+$ T cells (left) and data quantification across donor groups (right). Dotted lines represent median and interquartile range. Significance was determined using the Kruskal-Wallis

test with Dunn's correction (**a**), an unpaired t-test (**b**), or Welch's ANOVA with Benjamini-Hochberg correction (**c**). * $p < 0.05$, ** $p < 0.01$.

Figure 2. Cytolytic $CD8^+$ T cells are rare in the LNs of ECs. **a**, Representative flow plots showing perforin and granzyme B expression in LN-derived memory $CD8^+$ T cells (left) and data quantification across donor groups (right). **b**, Correlation between the frequency of perforin$^+$ granzyme B^+ LN memory $CD8^+$ T cells and pVL. Values for pVL below the limit of detection were plotted as 40 copies/mL. Significance was determined using Spearman's rank correlation. **c**, **d**, Representative immunohistochemistry images of LN biopsies (left) stained for perforin (**c**) or granzyme B (**d**) and data quantification across donor groups (right). **e**, Representative flow plots showing HIV-specific tetramer staining of LN-derived memory $CD8^+$ T cells (left) and data quantification across donor groups (right). Each dot represents a distinct tetramer$^+$ population in the quantification plot. **f**, Representative flow plots showing HIV-specific tetramer$^+$ cells (colored contours) overlaid on total LN-derived memory $CD8^+$ T cells (grey background) gated to display perforin and granzyme B expression (left) and data quantification across donor groups (right). Each dot represents a distinct tetramer$^+$ population in the quantification plot. **g**, Representative flow plots of redirected killing assays (left) and data quantification across donor groups (right). **h**, Representative flow plots showing CXCR5 expression on LN-derived memory $CD8^+$ T cells (left) and data quantification across donor groups (right). **i**, Quantification of CXCR5 expression on LN-derived tetramer$^+$ memory $CD8^+$ T cells. Each dot represents a distinct tetramer$^+$ population. **j**, Representative flow plots showing perforin and granzyme B expression in LN-derived $CXCR5^+$ and $CXCR5^-$ memory $CD8^+$ T cells (left) and data quantification across donor groups (right). Error bars represent median and interquartile range.

Significance was determined using the Kruskal-Wallis test with Dunn's correction (**a, c, d, e, f, h, i, k**) or a two-way ANOVA (**g**). * $p < 0.05$, ** $p < 0.01$, *** $p < 0.001$.

Figure 3. Distinct transcriptomic signatures characterize HIV-specific $CD8^+$ T cells from the LNs of ECs and CPs. **a**, Set-up of the scRNAseq experiment, including data exclusion criteria. **b**, tSNE visualization of the unsupervised kernel-based algorithm. **c**, Violin plots of cytolysis-related genes showing z-normalized expression levels. **d**, Average percent error of k-fold cross-validation of support vector machine (SVM) models using subsets of the L0-norm-ranked gene list. Each crossvalidation was reiterated 100 times. **e**, Heatmap showing z-normalized expression of the 200 feature genes. **f**, Gene ontology (GO) analysis of the feature gene list using topGO. The top 25 enriched terms were reported, and p-values were calculated using the classic Fisher method. **g**, tSNE feature plots showing the distribution of gene expression. tSNE coordinates were calculated using the first 50 principal components and iterated 1,000 times. The color gradient displays relative log-normalized gene expression levels. Significance was determined using scDD calculations (**c**, **g**). * $p < 0.05$, ** $p < 0.01$, *** $p < 0.001$.

Figure 4. Polyfunctionality is associated with protein translation efficiency in HIV-specific $CD8^+$ T cells from the LNs of ECs. **a**, Representative flow plots showing the production of TNF and IL-2 by HIV-specific $CD8^+$ T cells from the LNs of one EC and one CP in response to cognate peptide stimulation. Plots were pre-gated on total memory $CD8^+$ T cells. **b**, Quantification of cytokine production by HIV-specific $CD8^+$ T cells from LNs. The total response for each readout was determined by summing the corresponding frequencies after background subtraction of all Boolean gates using permutations of CD107a, IFNγ, TNF, MIP-1β, and IL-2. Error bars represent median and interquartile range. **c**, Polyfunctionality plot of HIV-

specific $CD8^+$ T cells from LNs. Only combinations of 4 and 5 functions are shown. Error bars represent mean and SEM. **d**, Pie charts summarizing all combinations of functions. **e**, Heatmap showing z-normalized expression levels of genes from the feature list identified by GO protein translation terms. **f**, Gene set enrichment analysis (GSEA) of the scRNAseq data with reference to the Reactome Pathway Database, reporting the top 10 enriched pathways in ECs and CPs. **g**, Quantification of protein translation efficiency in LN-derived $CD8^+$ T cells. LNMCs were incubated with HPG in methionine-free medium for 6 hours in the presence or absence of HIV-derived peptides or anti-CD3. Responding cells were defined using Boolean gating for $IFN\gamma^+$ and/or TNF^+ events. CM, central memory; EM, effector memory. Error bars represent mean and SEM. Significance was determined using a one-way ANOVA (**d**) or a two-way ANOVA (**b**, **g**). * $p < 0.05$, ** $p < 0.01$, *** $p < 0.001$.

ACKNOWLEDGMENTS

We thank the Virus and Reservoirs Core at the Penn Center for AIDS Research for assistance with viral quantification, the Pathology Core at the Hospital of the University of Pennsylvania for access to biopsy materials, Kajsa Noyan-Gertler for assistance with viral suppression assays, and Mingyao Li and Yan Che for initial contributions to the scRNAseq analyses. This study was funded in part by the Oregon National Primate Research Center National Institutes of Health (NIH) grant P51OD011092 and by federal funds from the National Cancer Institute under contract HHSN261200800001E. S.D., A.R., and D.C.D. were supported by the Intramural Research Program of the National Institute of Allergy and Infectious Diseases at the NIH. M.A.M., J.A.H., and M.R.B. were supported by the Penn Center for AIDS Research (P30

AI045008). M.A.M. was further supported by NIH R21 grant AI129636, the Campbell Foundation, and a grant from the W.W. Smith Charitable Trust (A1701). M.R.B. was further supported by NIH R01 grants AI076066 and AI118694 and the BEAT-HIV Delaney Collaboratory (UM1AI126620). D.A.P. was supported by a Wellcome Trust Senior Investigator Award (100326/Z/12/Z). The SCOPE cohort was supported by the University of California, San Francisco (UCSF)-Gladstone Institute of Virology and Immunology Center for AIDS Research (P30 AI027763), the Delaney AIDS Research Enterprise (AI127966), and the amfAR Institute for HIV Cure Research (109301). The content of this publication does not necessarily reflect the views or policies of the Department of Health and Human Services (DHHS), nor does the mention of trade names, commercial products, or organizations imply endorsement by the U.S. Government.

AUTHOR CONTRIBUTIONS

S.N., D.A.P., D.C.D., M.B., and M.R.B. conceptualized and designed experiments and wrote the manuscript; M.B. and M.R.B. supervised the study; S.N., A.S.J., and M.B. performed and analyzed flow cytometry experiments; C.D. and J.D.E. performed and analyzed RNAscope and immunohistochemistry experiments; E.G. and D.A.P. generated bespoke HLA class I tetramers; S.D., A.R., and D.C.D. performed scRNAseq experiments; S.N., S.D., D.T., D.A., and V.H.W. analyzed scRNAseq data; L.K.C. and M.A.M. performed viral quantification experiments; P.M.D.R.E., Y.A.T., A.N., G.R.T., and S.G.D. provided samples for the study.

COMPETING INTEREST STATEMENT

The authors declare no competing interests.

DATA AVAILABILITY

The sequencing data reported in this paper have been deposited in the Gene Expression Omnibus Database with the accession number GSE110684.

SUPPLEMENTARY MATERIALS

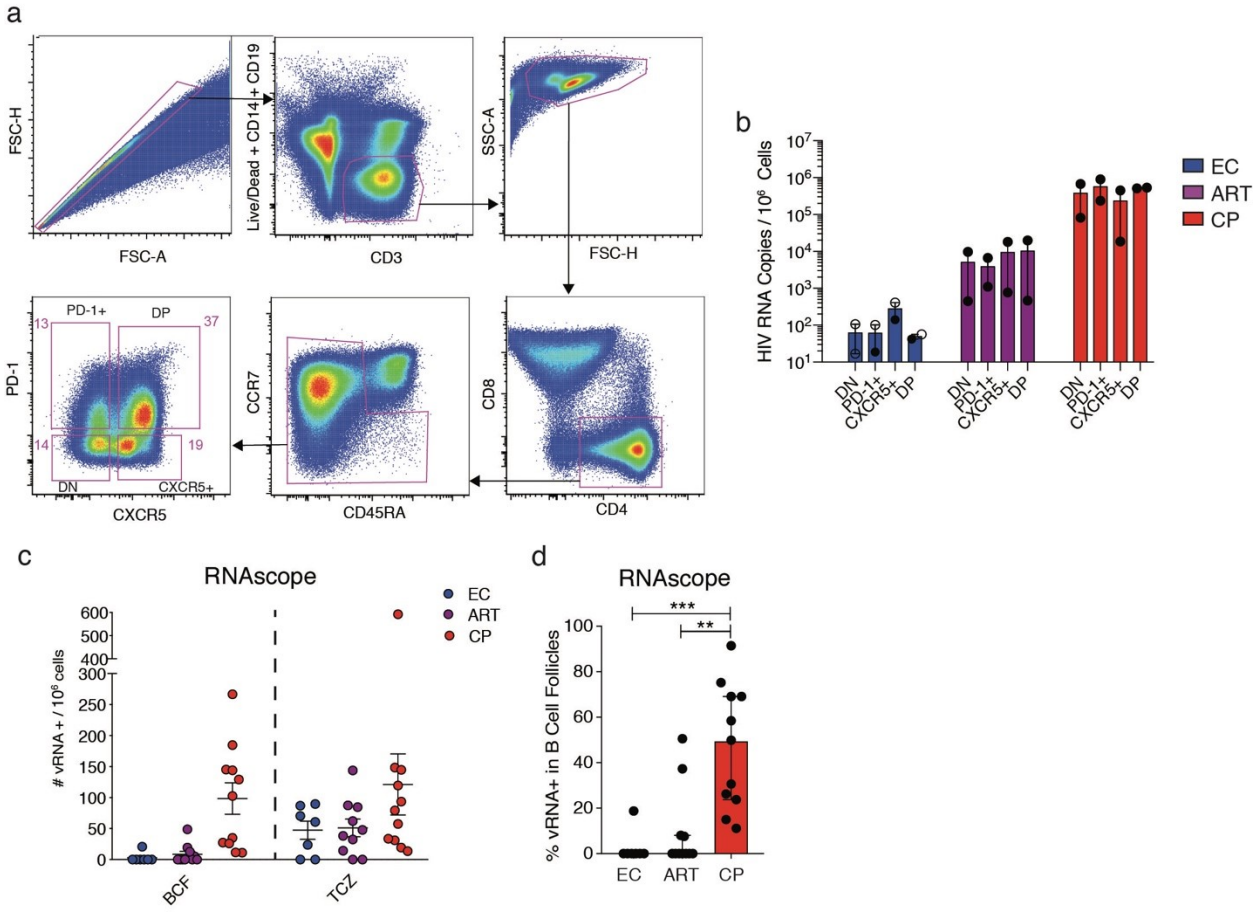

Supplementary Figure 1. HIV RNA is present in B cell follicles and the T cell zone in LNs. **a**, Gating scheme used to sort LN-derived $CD4^+$ T cell subsets for viral quantification. Representative flow plots were generated from the LNs of one EC. **b**, Quantification of HIV RNA in LN-derived $CD4^+$ T cell subsets by qPCR. The limit of detection value was used in the absence of detectable HIV RNA (open circles). **c,** Percent frequency of $vRNA^+$ cells in B cell follicles, as determined by RNAscope. Error bars represent mean and SEM (**b**) or median and interquartile range (**c**). Significance was determined using a two-way ANOVA (**b)** or the Kruskal-Wallis test with Dunn's correction (**c**). ** $p < 0.01$, *** $p < 0.001$.

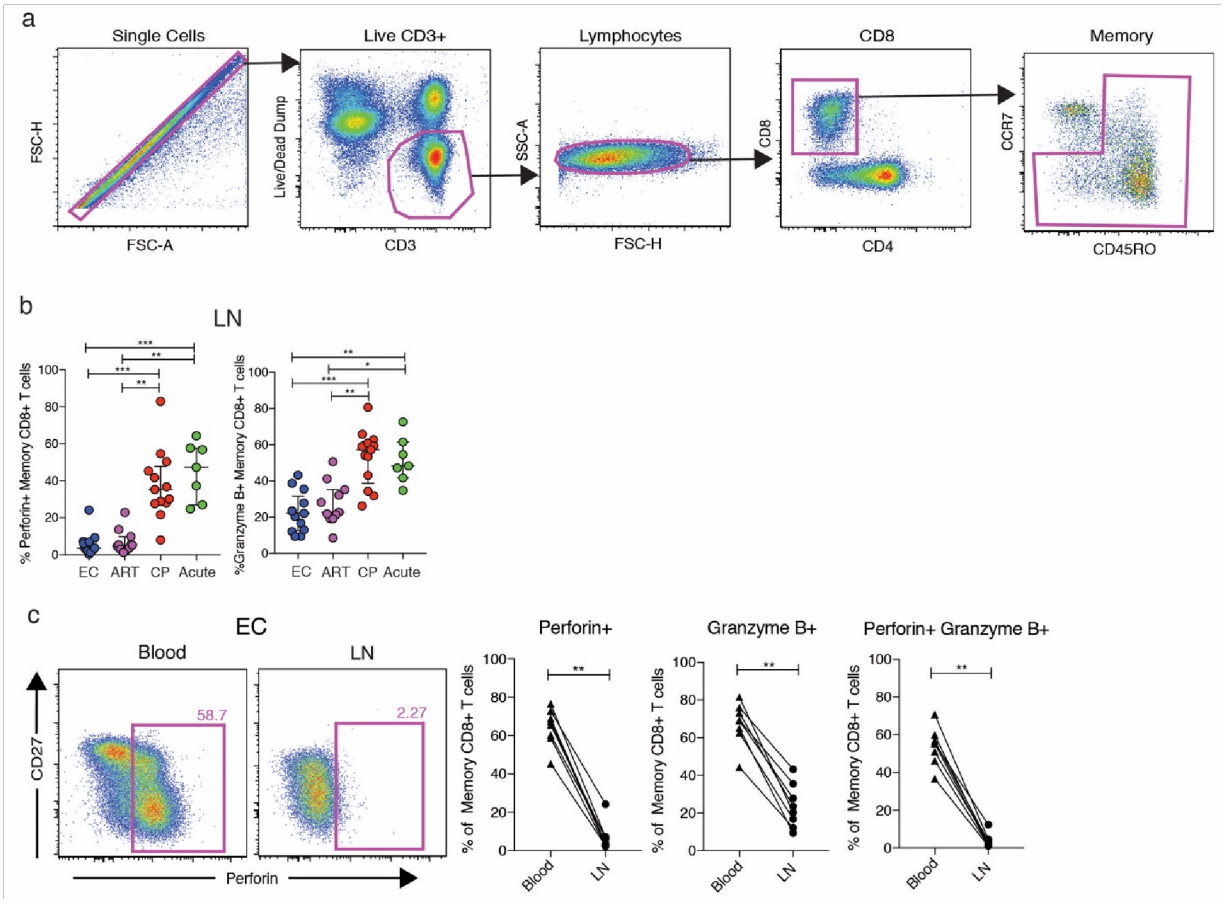

Supplementary Figure 2. $CD8^+$ T cells from the LNs of ECs express low levels of perforin and granzyme B. **a**, Gating scheme used in flow cytometry experiments. Representative plots were

generated from the LNs of one EC. All flow cytometry data shown in this report were pre-gated on memory $CD8^+$ T cells unless specified otherwise. **b**, Quantification of perforin and granzyme B expression in LN-derived $CD8^+$ T cells across donor groups. **c**, Representative flow plots showing perforin and granzyme B expression in matched peripheral blood and LN-derived $CD8^+$ T cells from one EC (left) and data quantification across donor groups (right). Significance was determined using the Kruskal-Wallis test with Dunn's correction (**b**) or the Wilcoxon matched pairs signed rank test (**c**). * $p < 0.05$, ** $p < 0.01$, *** $p < 0.001$.

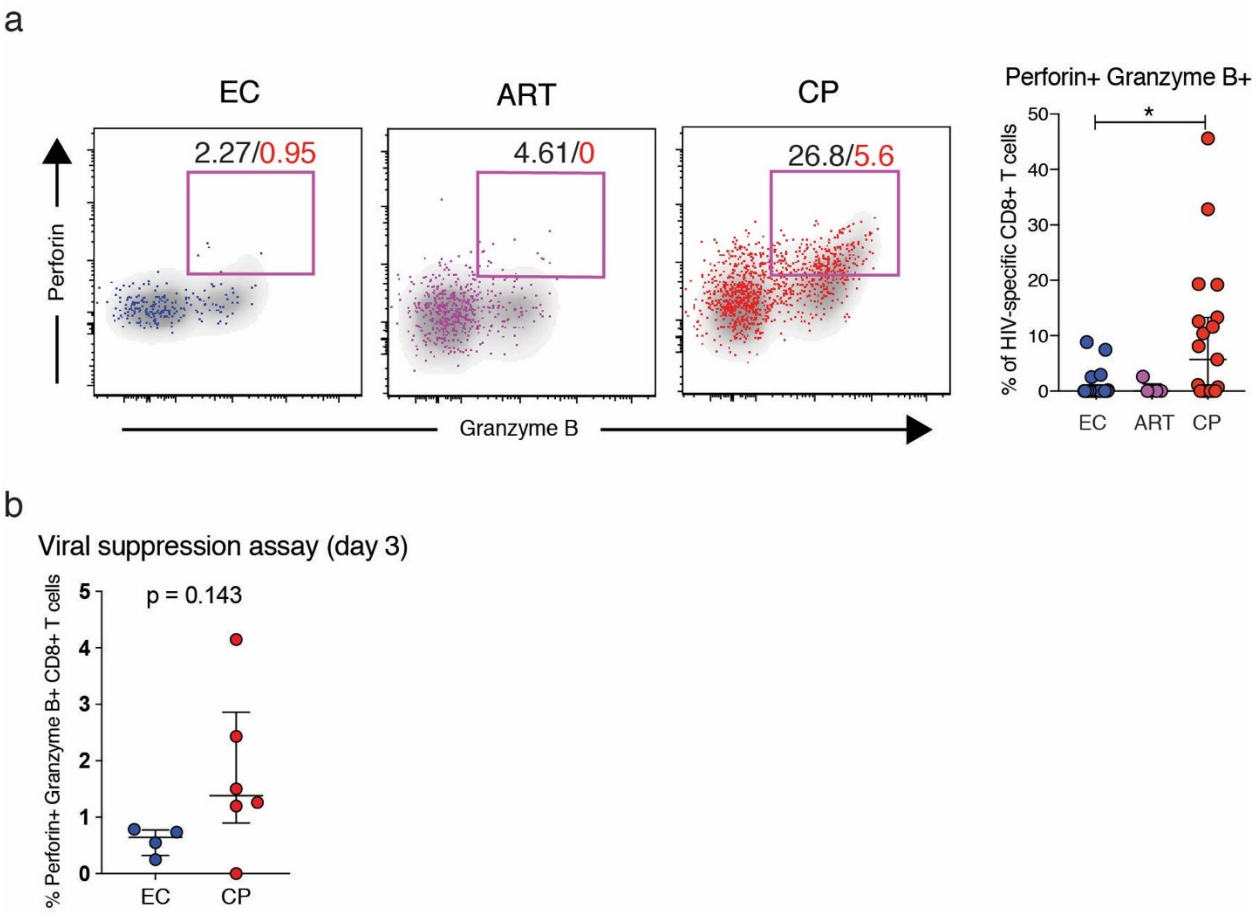

Supplementary Figure 3. $CD8^+$ T cells from the LNs of ECs do not upregulate cytolytic molecules in response to cognate antigen exposure. **a,** LNMCs were stimulated for 6 hours with peptides representing optimal epitopes derived from HIV. Perforin and granzyme B were

quantified in HIV-specific $CD8^+$ T cells. Colored dots in the representative flow plots (left) depict HIV-specific $CD8^+$ T cells defined by the expression of at least one of the following markers: CD107a, IFNγ, TNF, MIP-1β, or IL-2. Black and red numbers indicate the frequency of HIV-specific $CD8^+$ T cells before and after background subtraction, respectively. **b,** Frequency of LN-derived perforin$^+$ granzyme B^+ $CD8^+$ T cells after 3 days in culture with HIV-infected autologous LN-derived $CD4^+$ T cells, as shown in **Fig. 1c**. Significance was determined using the Kruskal-Wallis test with Dunn's correction (**a**) or an unpaired t-test (**b**). * $p < 0.05$.

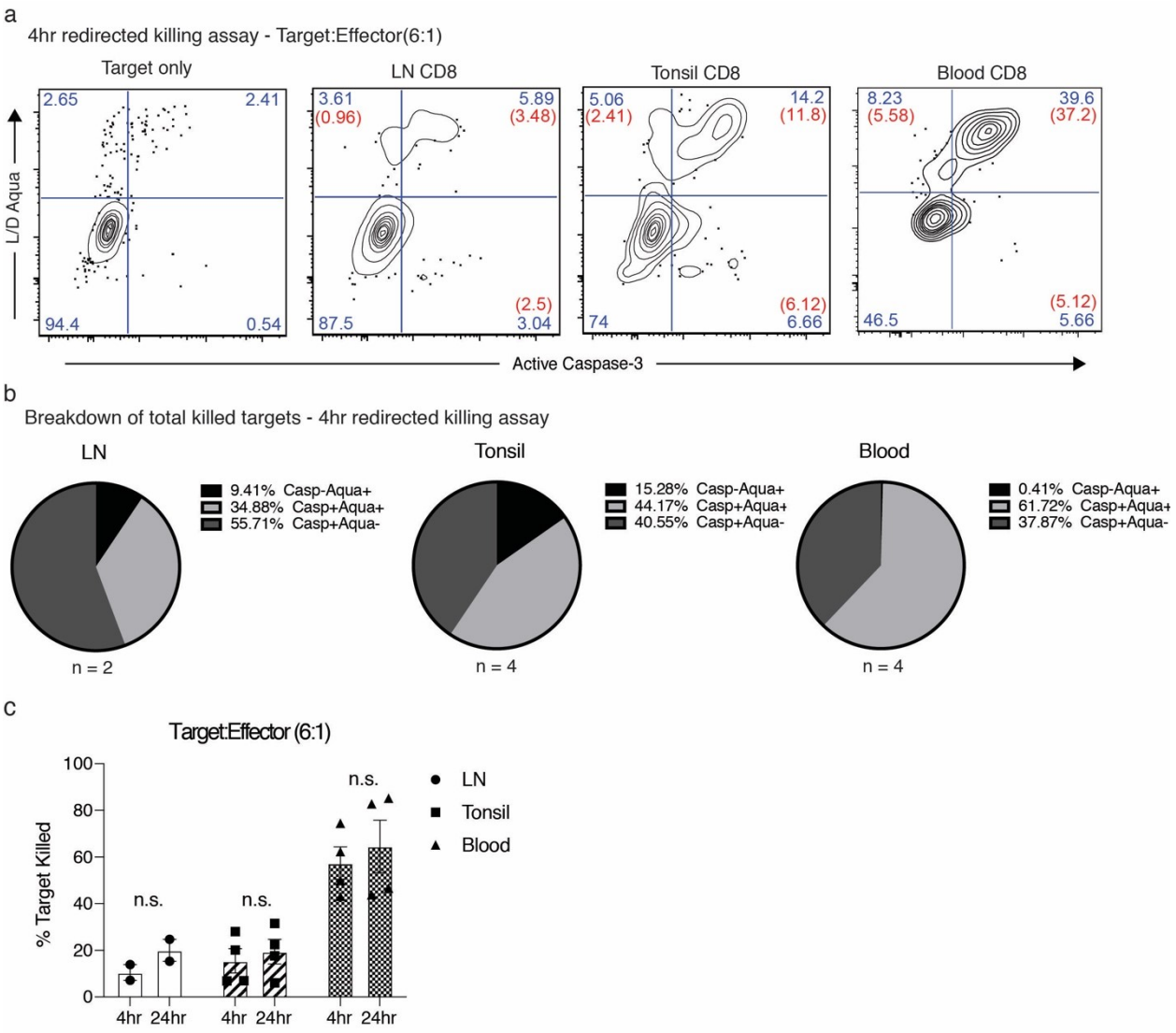

Supplementary Figure 4. Active caspase 3 detection captures the majority of killed target cells. $CD8^+$ T cells isolated from the LNs, tonsils, and peripheral blood of HIV^- individuals were incubated with anti-CD3-coated P815 cells at an effector:target ratio of 6:1 for 4 or 24 hours. **a,** Representative flow plots showing the detection of killed target cells via active caspase 3 *versus* LIVE/DEAD Aqua (L/D Aqua). Numbers represent frequencies of cells in each gate before (blue) or after background subtraction (red). **b**, Breakdown of the total killing after 4 hours. Casp, active caspase 3. Each pie chart represents total killing after background subtraction. **c,** Summary plot of redirected killing assays at 4 hours and 24 hours. % target killed represents the sum of $Casp^-Aqua^+$, $Casp^+Aqua^+$, and $Casp^+Aqua^-$ after background subtraction. Error bars represent mean and SEM. Significance was determined using a two-way ANOVA (**c**). n.s., not significant.

a

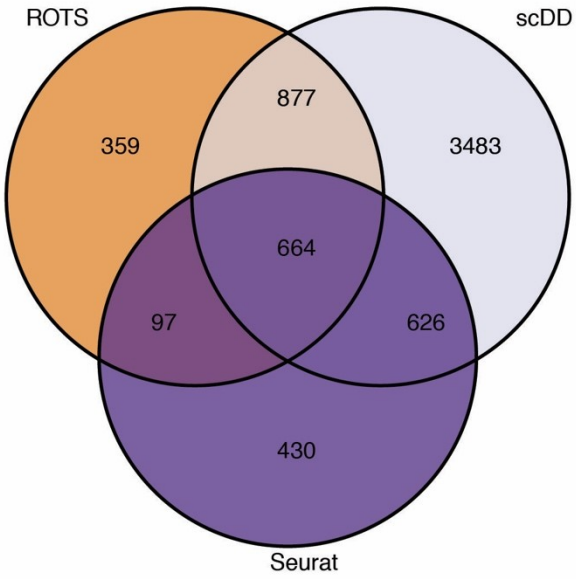

b

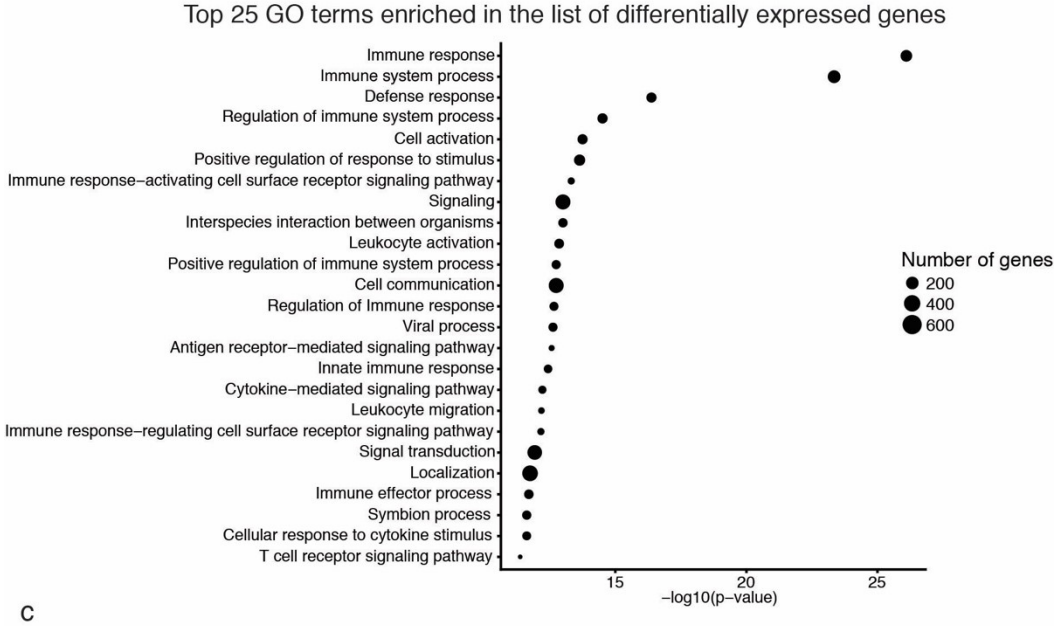

c

Secreted molecules that are upregulated in elite controllers via IPA analysis

Symbol	Gene Name	Expr p-value	Type(s)
IL32	interleukin 32	7.02E-09	cytokine
CCL5	C-C motif chemokine ligand 5	2.04E-04	cytokine
DDHD1	DDHD domain containing 1	2.94E-03	enzyme
IL1B	interleukin 1 beta	1.87E-04	cytokine
CXCL3	C-X-C motif chemokine ligand 3	1.17E-03	cytokine
CXCL2	C-X-C motif chemokine ligand 2	2.54E-03	cytokine
CCL2	C-C motif chemokine ligand 2	2.68E-03	cytokine
RNASE1	ribonuclease A family member 1, pancreatic	9.19E-03	enzyme
LTB	lymphotoxin beta	5.40E-05	cytokine
TNF	tumor necrosis factor	1.18E-09	cytokine
ADAMTS4	ADAM metallopeptidase with thrombospondin type 1 motif 4	1.32E-02	peptidase

Supplementary Figure 5. Differential expression analysis of the scRNAseq data. **a**, Venn diagram showing the overlap of differentially expressed genes detected by each of the three algorithms. A total of 2,264 genes achieved significance ($p < 0.05$) in at least two of the three algorithms. These genes are listed in **Supplementary Table 2**. **b**, The top 25 GO terms enriched among the 2,264 differentially expressed genes. **c**, List of secreted molecules that were upregulated in ECs, as determined by IPA. Expression p-values were derived from the scDD algorithm. Expr Log Ratio represents log fold-change values obtained from the ROTS algorithm; positive values indicate higher expression levels in ECs relative to CPs.

Supplementary Table 1. Clinical characteristics of donors included in this study. Values represent median and interquartile range.

	EC	ART	CP	Acute
Number	12	14	18	7
Site	San Francisco (USA)	San Francisco (USA), Philadelphia (USA), Mexico City (Mexico)	Mexico City (Mexico)	Mexico City (Mexico)
Age	52 (47-59)	40 (32-58)	31 (24-37)	23 (20-27)
Gender	10 Males / 1 Female / 1 Male to Female	8 Males / 1 Female / 5 No Info	10 Males / 1 Female / 7 No Info	7 Males / 0 Female
Viral Load (copies/mL)	<40	<40	51,396 (12,845-213,173)	1,996,027 (1,297,461-4,421,034)
CD4 Count	881 (660-1172)	544 (359-601)	348 (175-521)	306 (238-370)

Supplementary Table 2. Complete list of 2,264 genes that were differentially expressed between HIV-specific $CD8^+$ T cells from the LNs of ECs and HIV-specific $CD8^+$ T cells from the LNs of CPs. Expression p-values were derived from all three algorithms. Log fold-change values were obtained from the ROTS algorithm; positive values indicate higher expression levels in ECs relative to CPs.